LBL-11040

Lawrence Berkeley Laboratory
UNIVERSITY OF CALIFORNIA

MASTER

Invited lecture presented at the INS Kikuchi Summer School on Nuclear Physics at High Energies, Fuji-Yoshida, Japan, July 1-4, 1980

RELATIVISTIC NUCLEAR COLLISIONS: THEORY

Miklos Gyulassy

July 1980

Prepared for the U.S. Department of Energy under Contract W-7405-ENG-48

DISTRIBUTION OF THIS DOCUMENT IS UNLIMITED

RELATIVISTIC NUCLEAR COLLISIONS: THEORY*

Miklos Gyulassy

Nuclear Science Division
Lawrence Berkeley Laboratory
Berkeley, California 94720 USA

ABSTRACT

Some of the recent theoretical developments in relativistic (0.5-2.0 GeV/nucleon) nuclear collisions are reviewed. The statistical model, hydrodynamic model, classical equation of motion calculations, billiard ball dynamics, and intranuclear cascade models are discussed in detail. Inclusive proton and pion spectra are analysed for a variety of reactions. Particular attention is focused on how the complex interplay of the basic reaction mechanism hinders our attempts to deduce the nuclear matter equation of state from data.

DISCLAIMER

This book was prepared as an account of work sponsored by an agency of the United States Government. Neither the United States Government nor any agency thereof, nor any of their employees, makes any warranty, express or implied, or assumes any legal liability or responsibility for the accuracy, completeness, or usefulness of any information, apparatus, product, or process disclosed, or represents that its use would not infringe privately owned rights. Reference herein to any specific commercial product, process, or service by trade name, trademark, manufacturer, or otherwise, does not necessarily constitute or imply its endorsement, recommendation, or favoring by the United States Government or any agency thereof. The views and opinions of authors expressed herein do not necessarily state or reflect those of the United States Government or any agency thereof.

*Invited lecture at the INS Kikuchi Summer School on Nuclear Physics at High Energies, Fuji-Yoshida, July 1-4, 1980

I. INTRODUCTION

Since the early 1970's the field of relativistic nuclear collisions has been growing rapidly. Today there is a wealth of data[1] on inclusive reactions of the type

$$P + T \rightarrow F_1 + F_2 + X_M \tag{1}$$

for projectiles (P = p, d, C, Ne, Ar, Fe) with lab kinetic energies in the range 200-2000 MeV/nucleon, on a variety of targets (T = C, NaF, Ca, Pb, U). Typically, the momenta of only one or two fragments ($F_i = \pi$, K, p, d, t, α) are measured per event. However, the reaction is sometimes further specified by a global constraint on the unobserved fragments X. For example, a bias toward small impact parameter events can be achieved by requiring a high associated multiplicity M in a given tag counter array.

To uncover the physics behind this staggering variety of reactions and data, an equally vast variety of models have been proposed. The purpose of this report is to review some of the important theoretical ideas behind these models and to assess our current understanding of relativistic nuclear collisions. Essentially, this report is an updated version of a similar review[2] given two years ago. Other reviews can be found in Ref. 3.

There are two distinct roles theory plays in this field. The first role is to motivate and encourage experiments by presenting speculative calculations on what novel phenomena could arise in dense, highly excited nuclear matter. The second role is to disentangle the complicated "bread and butter" physics of the basic reaction mechanism. In the first area, a rich harvest of ideas have already been generated[4,5,6] ranging from abnormal nuclear states, pion condensates, to quark matter as possible new phases of dense nuclear matter. However, the problem with these calculations is that they deal in general with only static (equilibrium) properties of nuclear matter with no attempt made to address the dynamical problem of how these phases could show up in nuclear collisions. Here is where the second role of theory enters. Clearly, the basic reaction mechanism must be understood before we can interpret any feature of actual data as evidence for or against one of these possibilities. In the past two years

there has been substantial progress in classifying and clarifying the many complex details of the reaction mechanism. In this report, we shall concentrate on these accomplishments of theory.

I.1 Expectations, Hopes and Goals

To begin the discussion, we recall first the main expectations, hopes and goals of high energy heavy ion physics. In particular, what new physical domains can we expect the field to cover? What novel phenomena can we hope to observe? Finally, what are the goals as to the new physics we want to extract from heavy ion collisions?

At energies $E > 100$ MeV/nucleon, the relative nucleon velocities exceed typical sound velocities, $\lesssim c/3$, in nuclear matter, and hence, density pile-ups are expected to occur. Even in the absence of interactions, simple interpenetration would lead to double densities, $\rho = 2\rho_0$, $\rho_0 = 0.17\ \mathrm{fm}^{-3}$. With interactions, much higher densities, $\rho \gtrsim 4\rho_0$, can be reached in strong shock zones. However, such high densities can be attained only at the price of high excitation energies, $E^* \sim 50$-100 MeV/nucleon. Thus, we expect extreme conditions during heavy ion collisions with $\rho > \rho_0$ and $E^* > E_F$ = Fermi energy, that are far outside the realm of conventional nuclear physics ($\rho \leqslant \rho_0$, $E^* << E_F$).

One hope is that novel states of nuclear matter or unusual collective phenomena will manifest themselves under those extreme conditions. As the density increases, more nucleons come within the range of each others' forces. Long-range correlations can then develop resulting in phase transitions in nuclear matter. Model calculations in fact suggest that such phase transitions are likely to occur for $\rho \gtrsim 2\rho_0$. In particular, phase transitions leading to density isomers and pion condensates have been extensively studied.[4,5] Speculations[6] have also arisen suggesting that at high ρ, nucleons would lose their identity and merge into a new state of quark matter.

However, whether exotic phenomena occur or not, an important goal with nuclear collisions is to learn about the nuclear equation of state: $W(\rho,T)$ = energy per nucleon as a function of density and temperature. Incredibly, the only thing known about W today is that $W(\rho_0,0) = -16$ MeV and $\partial W/\partial\rho = 0$ at $(\rho_0,0)$. Even the incompressibility $K = 9\rho_0^2\partial^2 W/\partial\rho^2$ at $(\rho_0,0)$ is uncertain with

K ~ 150-400 MeV. The determination of $W(\rho,T)$ over any finite region of the (ρ,T) plane would thus vastly expand our understanding of nuclear physics.

I.2 Obstacles

There are, however, major obstacles in the way of determining $W(\rho,T)$ from nuclear collisions. The most significant one is that only asymptotic states can be observed experimentally. While the actual dynamical path in such collisions may depend on $W(\rho,T)$ over a wide range of ρ and T, only the final state of the dynamics is observed. In particular, there may be many different $W(\rho,T)$ that could lead to the same final energy and angle distributions. Another obstacle is that $W(\rho,T)$ makes sense only if local *equilibrium* is reached during the collision. Otherwise, we would also observe *transient*, non-equilibrium properties of the system as it evolves from the initial configuration toward equilibrium. Finally, heavy ion collisions involve *finite* systems where surface effects (curvature, diffuseness), not described by $W(\rho,T)$, are important. In order to assess the limitations imposed by these obstacles, we must turn to detailed model calculations of nuclear collisions.

II. CHOICE OF THEORETICAL FRAMEWORK

Before discussing the specific models though, we consider the question of which theoretical framework is expected to be appropriate for high energy heavy ion collisions.

II.1 The Ultimate and Less

A complete theoretical framework for relativistic nuclear collisions would have to be based on a complete relativistic quantum field theory of hadronic interactions. We have today a candidate for such a theory: Quantum Chromodynamics (QCD). In this non-Abelian gauge theory, hadrons are described by SU(3) color singlet quark states confined in a bag of radius $R_B \approx 0.3 - 1.0$ fm. The exchange of colored gluons mediates the force between quarks. The forces between color singlet hadrons are, on the other hand, short-range (non-local, non-static) van der Waals type forces involving quark interchange as shown in Fig. 1a. Unfortunately,

the large distance properties of QCD are not calculable at present and we are forced to introduce idealizations and simplifications.

For a nuclear system, the full complication of QCD is likely to be important only when the hadron bags overlap. This occurs either for high densities $\rho \gtrsim \rho_c \approx (4\pi R_B^3/3)^{-1} \sim (1\text{-}50)\rho_0$ or for high temperatures $T \gtrsim T_c = (1\text{-}2)m_\pi \sim (140\text{-}300)$ MeV. These estimates for ρ_c and T_c are, of course, very uncertain. For $\rho < \rho_c$, $T < T_c$ hadrons can be described approximately as structureless particles interacting via meson exchange, as shown in Fig. 1b. Excited states of hadrons, such as the Δ_{33} resonance, can be treated as distinct particles. While it is straightforward to write down Lorentz invariant effective Lagrangians for such a theory, the relativistic field equations are also intractable outside limited approximation schemes such as the mean field theory.[7]

To simplify the theory further we could try to neglect relativistic effects. This is justified below particle production thresholds $E_{lab} \lesssim 300$ MeV/nucleon. For these energies we may expect the N-body Schroedinger equation with static two-body potentials to be adequate. But alas, our computational capabilities fail us here too. Even the ground state of nuclear matter remains a formidable challenge after 40 years of Breuckner, e^s, and hypernetted chain attempts.

At the present then there is no calculable quantum theory of nuclear collisions. It is conceivable that within a few decades lattice theories, Monte Carlo simulations, and computer technology will have achieved the sophistication necessary for a full quantum calculation, but for now we must settle for less.

II.2 Classical Limit

The less is clearly classical mechanics: $\hbar = 0$. But is classical mechanics really so bad for nuclear collisions? The answer depends very much on the specific observable we have in mind. For example, diffractive elastic scattering, which accounts for about a half of the total cross section, is due to pure quantum shadowing effects. However, we generally observe only the reaction cross sections in nuclear collisions. One measure of the importance of quantum effects for these is the typical angular momentum in relativistic nuclear collisions:

$\langle L \rangle \sim PR \sim Am_N cR \sim 5A^{4/3}\hbar$. For Ar + Ar, for example, $\langle L \rangle \sim 700\hbar$, and thus very many partial waves are expected to contribute to any one channel. The interference terms in this case tend to average away and the modulus square of the partial wave sum can be safely replaced by classical integration over impact parameters, b. Thus, classical geometrical considerations are likely to apply quite well to such reactions.

For a fixed impact parameter, we can then ask how quantum effects can show up due to particular reaction dynamics. If nuclei were crystalline, then phase coherence could result in striking interference patterns in the final one-particle inclusive spectra. However, nuclei are much more like liquids, with particles moving in a uniform mean field. Hence the scattering centers are distributed approximately uniformly in the nucleus. After the ensemble average corresponding to all possible initial conditions, no interference pattern is likely to survive in the one-particle inclusive distribution. The obvious simple analogy is the two-slit Young's interferometer where the slit spacing is allowed to fluctuate on a scale Δd. For a beam of momentum k the interference pattern is washed away when $k\Delta d \gg 1$. For nuclei $\Delta d \sim \pi/p_F \sim 2$ fm, so that $k\Delta d \gg 1$ for $k \gg p_F \approx 250$ MeV/c. Thus for nuclear beams with $E_L > 100$ MeV/nucleon, such interference effects are negligible.

However, some quantum interference effects can survive in many-body observables. In particular, interference due to symmetrization or anti-symmetrization of the final wavefunctions for identical bosons or fermions can be observed even for such chaotic reactions. As first shown by Hanbury-Brown and Twiss, the two-particle coincidence experiment, which in optics is called *intensity interferometry* in contrast to Young's *amplitude interferometry*, can detect interference patterns arising from such quantum statistics effects. This type of final state quantum interference is, however, only important when the relative momentum $q = |p_1 - p_2|$ of the two identical particles is small. In fact, if R is the radius of the reaction zone, then $qR \lesssim \hbar$ is the necessary condition for such interference effects to occur. This is easy to see because for $qR \gg \hbar$ even indistinguishable particles become distinguishable since slight variations in R or q make the relative phase e^{iqR} vary wildly. Similarly for

an m-body inclusive measurement, quantum statistics interference is important only when some of relative momenta $q_{ij} = |p_i - p_j| \lesssim \hbar/R$.

It is also important to note that even for distinguishable particles such as p and n quantum effects can enter for small relative momenta due to final state interactions. The ground state of composite fragments such as d, α, etc., certainly involve quantum mechanics. The scale of relative momenta for which such final state interactions will be important is determined by the Fourier components of the composite wavefunctions. For nuclear fragments that scale, which is called the coalescence radius[14], is clearly $\sim p_F$. Thus when $q_{ij} \ll p_F$, quantum effects will be important even for unlike particles.

We conclude that quantum effects are likely to show up only in limited kinematic domains, $q_{ij} < 1/R$ or p_F, of multiparticle ($n \geq 2$) inclusive cross sections. They can indirectly show up in the single inclusive spectra if the probability of finding two particles within the coalescence radius is large. This occurs, for example, near the projectile and target fragmentation regions where there is the highest probability of finding composite fragments. For high energy nuclear collisions there is, however, a large region of momentum space of radius $\sim p_{cm}$ (center of mass momentum per nucleon) which is only sparsely occupied. In that region classical mechanics is likely to yield adequate results for inclusive cross sections. In fact, as we shall see, phase space and geometry are often enough to determine the gross features of the data in those regions.

II.3 Classical Methods

Once we adopt a classical approach tc nuclear collisions, the general framework for dynamical calculations is the Equation-of-Motion (EOM) method.[8] We are then restricted to energies $E_L \ll 1$ GeV/nucleon where relativistic kinematics and particle production can be neglected. Then it remains a numerical problem to solve Newton's equations for the classical trajectories as illustrated in Fig. 1c. The results of such calculations will be presented in Section III. However, it is instructive to note under what conditions EOM can be simplified.

Various approximations to EOM are possible depending on the time and length scales in the problem. We follow Bodmer[8] below.

For heavy ion collisions (E ~ 200-500 MeV/nuc) the following time scales are relevant:

1) τ_{int} = duration of individual NN collision
$= \text{force range } r/c$
$\approx 0(\hbar/m_\pi c) \sim (1\text{-}2)\ \text{fm/c}$

2) τ_{rel} = relaxation time between successive NN collisions
$= \frac{\lambda}{v} \sim \frac{2\ \text{fm}}{(1/2 - 3/4)c} \sim (3\text{-}4)\ \text{fm/c}$

3) τ_{col} = total collision time
$= \frac{L}{v} \sim \frac{10\ \text{fm}}{(1/2 - 3/4)c} \sim (10\text{-}20)\ \text{fm/c}$

Note that the pion mass sets the scale for τ_{int} because OPE is the longest range nucleon force. For τ_{col}, $L \sim 10$ fm is the typical nuclear dimension traversed in central collisions.

While there are no gross differences between these time scales, the following inequality does seem to hold:

$$\tau_{int} < \tau_{rel} < \tau_{col} \qquad (1)$$

Rigorous approximations to EOM would follow if any of the $<$ signs in Eq. (1) were replaced by $\ll$.

Consider the three possible cases:

A. $\tau_{int} \ll \tau_{rel}$

B. $\tau_{rel} \ll \tau_{col}$

C. $\tau_{int} \ll \tau_{rel} \ll \tau_{col}$

II.2(A) $\underline{\tau_{int} \ll \tau_{rel}}$: <u>The billiard ball limit</u>.

In case A, only isolated two-body collisions occur and collective effects are unimportant. This is the dilute gas limit. In this case EOM reduces to the *Boltzmann equation* or to *intranuclear cascade*, specified by free space NN cross sections.[9,10] Between collisions, the particles move in straight line trajectories

shown in Fig. 1d. In heavy ion collisions, the condition $\tau_{int} \ll \tau_{rel}$ is rather marginally satisfied, especially when we consider the possible density dependence of the force range, r. In free space $r \sim \hbar/m_\pi c$, but in nuclear matter collective effects (polarization) can enhance r by a factor ~2 for $\rho \gtrsim 2\rho_0$ (see Ref. 4).

II.2(B) $\tau_{rel} \ll \tau_{col}$: The hydrodynamic limit.

In case B, sufficiently many two-body scatterings occur during the collision time that *local thermal equilibrium* can be assumed during the collision. In that case, EOM reduces to *hydrodynamics*[11] where nuclear interactions, binding and collective effects are described through an equation of state $W(\rho,T)$. The condition $\tau_{rel} \ll \tau_{col}$ is best (although again marginally) satisfied for central collisions. Furthermore, in some regions of the interaction zone (within a mean free path of the surface) $\tau_{rel} \sim \tau_{col}$ even for heavy systems. In that case hydrodynamics may apply only to the interior regions.

II.2(C) $\tau_{int} \ll \tau_{rel} \ll \tau_{col}$: The phase space limit.

Finally, the greatest simplification of EOM occurs in case C. In that case, EOM reduces to hydrodynamics with an ideal gas equation of state. There are then no compression effects and the excitation energy is distributed into translational and thermal energy. Clearly, this case has the greatest potential with regard to formulating simple *analytic* models for heavy ion collisions.[12,13] Unfortunately, the necessary condition $\tau_{int} \ll \tau_{rel} \ll \tau_{col}$ is also not well satisfied in Eq. (1).

II.3 The Need for a Variety of Models

Therefore, we are faced with the following dilemma: among all the tractable approaches that are possible in cases A, B, and C, none can be rigorously justified for heavy ion collision. Note, however, that Eq. (1) does not rule out at least the partial validity of any of those approaches. Thus, the gross features of the data may turn out to be qualitatively reproduced, but the magnitude of the errors inherent in the methods cannot be estimated ahead of time. Recall also that this whole discussion was restricted to the non-relativistic case where particle production

is negligible. For E > 500 MeV/nuc, additional model assumptions will have to be made to incorporate π production.

Since no rigorous theoretical framework could be found for relativistic nuclear collisions, the best way to proceed is to turn to model calculations that include as many "realistic" effects as possible. The philosophy must then be shifted from seeking perfect agreement with data to providing *background* calculations that reveal the importance of particular (calculable) aspects of the dynamics. By varying the parameters within the models and by comparing results of different models, the sensitivity of the predictions to specific details can be determined. In this way, the most essential elements of the dynamics can be hopefully isolated. Therefore, we turn in the next section to the consideration of a variety of dynamical models collected together in the extended Zoo of Models. The next section provides a guided tour of that zoo.

III. THE ZOO OF MODELS

In the past two years there has been a population explosion in the zoo as evidenced by all the new faces in Refs. 8-13. It is now an increasingly difficult task to keep track of all the beasts and hybrids. Rather than assign each new paper a cage of its own, I will invoke the zookeepers perogative of displaying only a few choice examples of each species. I apologize in advance to those owners whose pets have not been adequately or properly represented. Also, rather than follow the historical order of model development – who begat whom (an exercise left to the ardent reader of Refs. 8-14) – I will take advantage of hindsight in organizing the discussion.

III.1 Statistical Phase Space Models

In this section we follow closely the work of Knoll and collaborators.[12,13]

The first important step in constructing simple models[12,13] of nuclear collisions is the separation of geometrical and dynamical effects. As we argued in Section II, classical geometrical concepts should be applicable for such reactions. For a fixed impact parameter $\underset{\sim}{b}$, it is then natural to divide the nucleons

into groups of participants and spectators as illustrated in Fig. 2a. We expect the participants of the collision to involve those nucleons in the geometrical overlap region of the two nuclei as they sweep past one another.

However, a particular nucleon in the projectile will interact most likely with only a few nucleons in its path. If the momentum of the incident nucleon is sufficiently large, $p_L \gtrsim 1$ GeV/c, then because NN reactions have a limited perpendicular momentum distribution ($d\sigma/dt \propto e^{-bt}$, $b \sim 6(\mathrm{GeV/c})^{-2}$, $t = (p_1 - p_2)^2$) the trajectory of the nucleon through the nucleus can be approximated by a straight line. This is the basic Glauber hypothesis.[12.1] In that case the *average* number of collisions a nucleon will suffer traversing a nucleus A at impact parameter $\underset{\sim}{s}$ is[12]

$$\bar{N}_A(\underset{\sim}{s}) = \int dz\ \rho_A(z,\underset{\sim}{s})\ \sigma_{NN} \tag{5}$$

where ρ_A describes the diffuse nuclear density. However, there is also Poisson probability that it will actually suffer n collisions:

$$P_A(n,\underset{\sim}{s}) = e^{-\bar{N}_A(\underset{\sim}{s})}\ \frac{(\bar{N}_A(\underset{\sim}{s}))^n}{n!} \quad . \tag{6}$$

This is due to possible fluctuations in the number of nucleons in its path. In a nuclear collision with a fixed impact parameter $\underset{\sim}{b}$, the probability that m nucleons from the projectile A scatter with n nucleons along their path at a relative impact parameter $\underset{\sim}{s}$ in the target B is then just $P_A(m,\underset{\sim}{b}-\underset{\sim}{s})P_B(n,\underset{\sim}{s})$. Each such tube-tube collision contributes σ_{NN}, to the reaction cross section. Therefore the net contribution to the reaction cross section from collisions involving m + n nucleons is

$$\sigma_{AB}(m,n) = \sigma_{NN} \int \frac{d^2b}{\sigma_{NN}}\ \mathcal{B}(\underset{\sim}{b}) \int \frac{d^2s}{\sigma_{NN}}\ P_A(m,\underset{\sim}{b}-\underset{\sim}{s})\ P_B(n,\underset{\sim}{s}) \ , \tag{7}$$

where $\mathcal{B}(\underset{\sim}{b})$ is the distribution function for impact parameters. With $\mathcal{B}(b) \equiv 1$, corresponding to no restriction of impact parameters, σ_{AB} factorizes as

$$\sigma_{AB}(m,n) = \frac{\sigma_A(m)\ \sigma_B(n)}{\sigma_{NN}} \tag{8}$$

where $\sigma_A(m) = \int d^2s\ P_A(m,s)$.

Knowing the relative weights of m on n collisions, we can then write the invariant single nucleon inclusive cross section as[12,13]

$$\sigma_I(\underset{\sim}{p}) = \varepsilon_p \frac{d^3\sigma}{dp^3} = \sum_{m,n} \sigma_{AB}(m,n)\ F_{m,n}(\underset{\sim}{p}) \ . \tag{9}$$

In Eq. (9) all the geometrical considerations have been isolated in σ_{AB} via Eq. (7). What remains to be specified is the dynamics leading to the Lorentz invariant distribution $F_{m,n}(\underset{\sim}{p})$. Clearly, F must involve a 3(m+n-1) dimensional momentum integration over the unobserved momenta of the remaining m+n-1 nucleons. Also,

$$\int \frac{d^3p}{\varepsilon_p}\ F_{m,n}(\underset{\sim}{p}) = m+n \tag{10}$$

by baryon conservation. In general, we expect $F_{m,n}$ to be of the form

$$F_{m,n}(\underset{\sim}{p}_1) = \int \frac{d^3p_2}{\varepsilon_2} \cdots \frac{d^3p_{m+n}}{\varepsilon_{m+n}}\ |S(\underset{\sim}{p}_1, \underset{\sim}{p}_2, \ldots, \underset{\sim}{p}_{m+n})|^2\ \delta^4\Big(\sum_1^n p_i - P_{mn}\Big) \tag{11}$$

where P_{mn} is the incident four momentum of the m+n system and $|S|^2$ describes the exclusive probability for final states $\underset{\sim}{p}_1, \ldots, \underset{\sim}{p}_{m+n}$. Unfortunately, we cannot calculate the S-matrix from first principles at this time.

The simplest model assumption about the dynamics we can make is that it is the most complicated possible! That means that there is equal probability of populating all accessible states, i.e., those states that lie within kinematic boundaries determined by $\delta^4(\Sigma\, p_i - P_{mn})$ in Eq. (11). This is the essence of the Fermi statistical theory[13.8] that has been applied to nuclear collisions by Knoll.[13.5-7] In that case $|S|^2$ is replaced by a constant (1/number of accessible states), leaving $F_{m,n}(\underset{\sim}{p})$ proportional to the Lorentz Invariant Phase Space (LIPS) integral $\phi_{m+n}(s')$, where

$$\phi_n(P^2) = \int \frac{d^3p_1}{\varepsilon_1} \cdots \frac{d^3p_n}{\varepsilon_n}\ \delta^4\Big(\sum_1^n p_i - P\Big) \ . \tag{12}$$

Therefore, the statistical model for nuclear collisions is specified by two elements, (1) the invariant single inclusive distribution given by

$$F_{m,n}(\underset{\sim}{p}) = (m+n)\,\frac{\phi_{m+n-1}((P_{mn}-p)^2)}{\phi_{m+n}(P_{mn}^2)}\,, \qquad (13)$$

and (2) the geometrical input of Eq. (7). For $m+n \gg 1$ and in the non-relativistic limit ($\varepsilon_i = m + p_i^2/2m$), Eq. (13) reduces to the familiar thermal limit[13.1-3]

$$F_{m+n}(\underset{\sim}{p}) \xrightarrow[m+n \gg 1]{} (m+n)\,\frac{e^{-(\underset{\sim}{p}-\underset{\sim}{p}_{mn})^2/2mT_{mn}}}{(2\pi\, mT_{mn})^{3/2}}\,, \qquad (14)$$

where p_{mn} is the center of mass momentum per nucleon, and $3/2\ T_{mn} = E^*_{mn}$ = center of mass energy per nucleon.

With Eq. (14) used in Eq. (9), we recover the firestreak model[13.2,13.3] as illustrated in Fig. 2b. The simpler fireball model[13.1] is recovered with the further assumption that for each impact parameter complete thermalization between adjacent tubes is reached as well, i.e., when velocity and temperature gradients are neglected in the interaction zone and the total phase space of *all* participants is considered.

The statistical model has the distinct advantage over thermal models of including finite number effects via Eq. (13). In Fig. 3a the differences between Eq. (13) and (14) are illustrated. Finite particle phase space is suppressed both in the low and high energy domains relative to the thermal limit. Support for this finite particle effect is seen in Fig. 3b for the $\theta_{cm} = 90°$ proton yield.[15.1] The statistical model predictions have been averaged over the Fermi momenta of the participating nucleons.[13.5] An alternative explanation of the shouldering feature of these spectra has been proposed in terms of the exploding fireball (or blast wave) model of Ref. 11.18. However, since the statistical model can account for that feature, the shoulder is not compelling evidence for a blast wave. On the other hand, the observed difference between the asymptotic slopes of the pion and proton spectra addressed in Ref. 11.18 cannot be explained by the statistical model.[13.7]

A more detailed comparison with data is given in Fig. 4. As we see, the gross features of the data are well reproduced. In Fig. 4b we see that even for the high multiplicity selected events,

the statistical model with $B(\underline{b}) = b^2(\underline{b})$ in Eq. (7) matches the data. The large anisotropy in the cm frame reflects the large shear velocities between adjacent tubes in Fig. 2b. This rules out the simple fireball model for such reactions. In Fig. 4c the qualitative features of the two proton coincidence rate are also accounted for. These data show that in certain regions of phase space there is a substantial non-equilibrium ($m = n = 1$ in Eq. (9)) component in collisions of light nuclei.

Having described the successes of the statistical model, we now list its limitations. First, the assumption of straight line trajectories will break down at low bombarding energies, $E_L \lesssim 500$ MeV/nucleon. This effects the relative weights of the clusters m,n in Eq. (9). Second, statistics cannot apply near the projectile and target fragmentation regions where the density of particles in phase space is so high that a large number of composites are formed. That is why this model has only been applied to the high cm energy data of Nagamiya et al.[15.1]. Third, for $E_L > 1$ GeV/nucleon pion production must be included. While the statistical model extended[13.7] to include pion production gives a good description of the shapes of the observed spectra, it has met with difficulties in accounting for the average pion multiplicity (see Ref. 13.7). Fourth, final state interactions such as Coulomb and spectator shadowing are not incorporated. Thus, for example, the in-to-out of plane correlation in Fig. 4c is predicted for heavy systems to be 1.0 whereas recent data[15.2] show it to be less than unity, ~0.9, presumably due to nuclear shadowing.

Even with these limitations we see that the statistical model provides a useful tool for background calculations. In particular, it shows which kinematic regions are dominated by geometry and phase space and which by dynamics. What we have learned is that most of the high momentum data can be understood in terms of simple geometry and phase space. Conversely, it will be difficult to learn dynamical details associated with the high density nuclear interaction zone from such data.

The statistical model also provides a convenient bridge between two extreme assumptions: the knock-out models[10] and thermodynamic models.[13] A knock-out model is defined by the assumption that all nucleons suffer at most a single hard

collision with another nucleon. Hard means that one or both of the nucleons had a high virtual momentum just prior to the collision. Typically, Fermi distributions with long exponential tails are needed to reproduce data.[10] Thus in the knock-out picture all high momentum components in the spectra arise because of *initial state* interactions between a group or cluster of nucleons in the target or projectile. Thermal, or more generally, cascade models, on the other hand, achieve the same high momentum components as a result of multiple scattering processes (intermediate state interactions) between groups of nucleons. In a statistical model there can, of course, be no distinction between initial, intermediate, and final state interactions. Only the number of nucleons that share their energy and momentum is considered *regardless* of the time ordering of the actual process. The success of a statistical model just means that for each group of m+n nucleons the interactions were sufficiently complex so that the final products sample uniformly the available multiparticle phase space. This perhaps provides a clue as to why the knockout picture with exponential Fermi distributions sometimes yields similar results to thermal models for one-body observables. In those cases the data simply reflect multiparticle phase space.

III.2 Hydrodynamics

While the statistical model accounts for the general features of the high momentum component of inclusive spectra for incident energies $\gtrsim$ 1 GeV/nucleon, it fails to reproduce the data at lower bombarding energies. For example, Ne + U at 400 MeV/nucleon cannot be understood in terms of geometry and phase space alone. We may therefore expect that this type of reaction contains more dynamical information than those shown in Figs. 3,4.

In this section we discuss whether hydrodynamics can describe nuclear collisions at energies ~500 MeV/nucleon. This question is of central importance because hydrodynamics provides the only direct link between data and the nuclear equation of state, $W(\rho,T)$. Recall that one of our main hopes was to deduce $W(\rho,T)$ via nuclear collision. We shall concentrate on the comparison of the latest data on central Ne + U (400 MeV/nucleon) collisions[15.3] with the most recent hydrodynamics calculations.[11.6]

This will allow us for the first time to draw rather strong conclusions on the difficulty of deducing $W(\rho,T)$ from data.

First, we recall the basic equations that underlie hydrodynamics.[11] These are the continuity of baryon number density ρ, momentum density $\underset{\sim}{m}$, and energy density e:

$$\frac{\partial}{\partial t}\begin{pmatrix}\rho\\ \underset{\sim}{m}\\ e\end{pmatrix} + \underset{\sim}{\nabla}\cdot\begin{pmatrix}\underset{\sim}{v}\rho\\ \underset{\sim}{v}\underset{\sim}{m}\\ \underset{\sim}{v}e\end{pmatrix} = \begin{pmatrix}0\\ -\underset{\sim}{\nabla}P\\ -\underset{\sim}{\nabla}\cdot(\underset{\sim}{v}P)\end{pmatrix} , \tag{15}$$

where $\underset{\sim}{v}(\underset{\sim}{x},t)$ is the flow velocity field and $P = \rho^2\, \partial W(\rho,T)/\partial\rho$ (at constant entropy) is the pressure.

Equation (15) is the simplest form of hydrodynamics where dissipative effects are neglected. Such effects become important when the gradient of some field quantity, $f(\underset{\sim}{x},t)$, is comparable to the mean free path λ. Corrections to Eq. (15) to order $\lambda|\nabla f|/f$ lead to the Navier Stokes equations, involving the viscoscity and thermal conductivity transport coefficients.[11.9-11.14,11.16] However, at this time the numerical uncertainties associated with solving the Navier Stokes equations are very large. Thus, while very suggestive pictures of hydrodynamic flow patterns have been generated, (see for example Fig. 5) the numerical uncertainties of the computed double inclusive cross sections $d\sigma/d\Omega dE$ (Fig. 5b) are too large to make possible a meaningful comparison with data.

The Euler equation (15) have been, on the other hand, solved to greater accuracy.[11.6] The input to these calculation is the nuclear equation of state, $W(\rho,T)$, for which the following assumption on the temperature dependence was made:

$$W(\rho,T) = W_o(\rho) + I(\rho,T) . \tag{16}$$

The internal energy I is assumed to be of the form appropriate for a nonrelativistic Fermi gas. The pressure in Eq. (15) is then given by $P = \rho^2\partial W_o/\partial\rho + 2/3\ \rho I$. In Eq. (16), W_o is the compression energy at zero temperature. For comparison, three models of W_o were considered as illustrated in Fig. 6. The curve for compressibility K = 200 represents a reasonable guess for W_o. Also shown are examples of a rather stiff equation of

state with $K = 400$ and a very soft equation of state with a density isomer at $\sim 3\rho_o$.

Before comparing with data, we note that composite fragment production is not correctly treated via hydrodynamics due to poor surface properties of the later. Thus, the fraction of protons that emerge in composite fragments cannot be calculated in this framework. We can however define a *charged particle* inclusive cross section by summing over the inclusive cross sections, $d\sigma(Z,N)$, for composites with Z protons, N neutrons as follows:

$$\varepsilon \frac{d^3\sigma}{d^3p} \text{ch} = \sum_{Z,N} Z \, \varepsilon \frac{d^3\sigma}{d^3p} (Z,N) \tag{17}$$

where (ε,p) is the same energy-momentum *per nucleon* for all fragments in the sum. Underlying Eq. (17) is the assumption that composite fragments are produced via final state interactions, after the violent phase of the collision. Thus, $d\sigma_{ch}$ is thought to represent the "primordial" distribution of protons, before coalescence[14.1] into light composites occurs. With this assumption, the distribution of charges obtained by solving Eq. (15) can be compared with the charged particle inclusive data.

The difference between $d\sigma_{ch}$ and $d\sigma(1,0) = d\sigma_p$ is largest for laboratory energies $E \lesssim 50$ MeV and forward angles. It is also important to remember that for heavy systems there can be large Coulomb distortions of the spectra, the magnitude of which is determined by $Z\alpha/RE$. Thus for U targets Coulomb distortion can modify the spectra by over 50% for $E \lesssim 40$ MeV. For $E \gtrsim 50$ MeV, both composite production and Coulomb effects are not so important, and therefore it is in this region where hydrodynamics should agree best with the Ne(400 MeV/nucleon) + U data.

For the impact parameter averaged inclusive spectra we see in Fig. 7 that the hydrodynamic calculations[11.6] provide, in fact, a reasonable description of the data[15.4] for $E \gtrsim 50$ MeV. However, within numerical uncertainties there also appears to be very little sensitivity to the three equations of state (Fig. 6) studied. A similar insensitivity of the single particle inclusive cross section to the equation of state was found in

Ref. (11.15). The calculations in Ref. (11.6) still do not include the final thermal averaging for each fluid cell, and only the flow velocities have been used to calculate $d\sigma_{ch}$. In a one dimensional example, thermal averaging was found to reduce the small sensitivity to the equation of state to a large extent.[11.6b] This was also anticipated in Ref. (11.15). As we shall see in the next section, classical equations of motion and billiard ball calculations also demonstrate the great insensitivity of the inclusive spectra to the equation of state. It is also worth mentioning that it appears[11.6] to be extremely difficult with current computer technology and techniques to reduce the numerical uncertainties in the hydrodynamical calculations.

Thus, our first conclusion is that $W(\rho,T)$ cannot be deduced from the impact parameter averaged $d\sigma_{ch}$. How about central collisions?

The first data on central collisions are now available[15.3,15.5] (See Fig. 8). Central collisions are defined by a cut on the associated multiplicity distribution corresponding to the highest 15% of the multiplicity distribution. From detailed intranuclear cascade[9.7] calculations (see Fig. 9), this multiplicity cut corresponds to the range of impact parameters $b < b_{max} = 4 \pm 1$ fm. For Ne+U the fraction of the reaction cross section from impact parameters less than b_{max} is $(4/11)^2 \sim 15\%$. Therefore, the hydrodynamic results integrated upto $b_{max} = 4$ fm should be comparable with the data of Ref. (15.3).

This comparison is shown in Fig. 8. Note first that there appears to be more sensitivity to the equation of state for central collisions. For example, at 30° the cross section falls off with energy slower for the softer $W_o(\rho)$, and at back angles there seem to be fewer low energy particles for the stiffer equation of state. Qualitatively we may attribute these effects to more complete stopping of Ne for the stiffer equation of state. For infinite stiffness, there would be no yield at 30° for central collisions while in the backward hemisphere high energy Ne fragments that bounced off the stiff U would be seen. Thus even with the large numerical uncertainties the qualitative trend of the calculations can be understood. We note again that thermal averaging would reduce the differences between the three cases.[11.6]

The most important point to note in Fig. 8 is that all three equations of state lead to large systematic deviations from the data. The main failure is the shape of the energy distribution at 30°. Even discarding the $E < 50$ MeV region where binding and Coulomb effects are important, the predicted energy dependence falls off much more rapidly with energy than does the data. In fact, the experimental shape of the 30° spectrum is very similar to the impact parameter averaged one in Fig. 7. At backward angles on the other hand, the $K = 200$ equation of state comes closest to the data although the numerical uncertainties are quite large. The data indicate that there are more protons with high velocity in the forward direction and less protons in the backward hemisphere.

This feature of the data suggests that there is less energy loss of the incident nucleons than predicted by hydrodynamics. Even with the generous variation in the equation of state and a generous allowance for numerical uncertainties, the comparison in Fig. 8 points to a serious inadequacy of 1-fluid hydrodynamics for this reaction. In Fig. 7, the impact parameter averaging must have helped camouflage this systematic deficiency.

We cannot argue that some other observable (such as the $n \geqslant 2$ particle inclusive cross section) may be better reproduced by hydrodynamics. If it fails at the single inclusive level, then it must fail for more exclusive observables.

The significance of Fig. 8 is that it demonstates for the first time that the *direct* link between $W(\rho,T)$ and the data is very weak. There must be physics in addition to $W(\rho,T)$ that is important even for these central collisions.

We already have a clue from the statistical model of the last section that finite particle number effects (granularity) may be important in nuclear collisions. Obviously, the basic assumption of hydrodynamics (see Sect. II.2(b)) that the mean free is very much smaller than the nuclear dimensions is not completely satisfied. If we look at Fig. 5 again for the geometry of Ne+U collisions at impact parameter $b = 4$ fm, we can guess what is the problem. A substantial number of the Ne nucleons still traverse the U in the surface region. From Eq. (5) it is clear that the number of mean free paths for those nucleons is not large. For nucleons at smaller relative impact parameters, on

the other hand, there will be ~7 mean free paths as they traverse the center of U. For these nucleons the assumption of local equilibration should be quite good. However, for the ones traversing the surface regions, hydrodynamics is likely to be a rather poor approximation. These nucleons will lose much less energy in the few collision they suffer than if local equilibration is assumed, and consequently they will be observed with higher energy in the forward direction. This finite mean free path effect will also result in less backward proton yield. Therefore, it is suggestive that the failure of hydrodynamics is due to just this finite number effect. In this regard, data with symmetric projectile, target combinations should exhibit larger deviations from hydrodynamic behavior because there are always more surface regions involved in such collisions at any impact parameter.

To reduce this finite number effect it would clearly be desirable to isolate even more central ($b \lesssim 2$) collisions (complete diving of Ne into U). However, the intranuclear cascade calculations[9,7] show in Fig. 9 that the average associated multiplicity in a Ne+U collision does not change very much between $b = 0$ and 4 fm due to simple geometrical effects. Thus, we cannot hope to isolate more central collisions simply by triggering more severely on the associated multiplicity distribution. Perhaps the azimuthal distribution of final fragments could be used to restrict further the range of impact parameters, but likely the large dispersion of the azimuthal distribution for fixed impact parameters will also make such a trigger scheme ineffective. We need new ideas for isolating truly central events with $b < 2$ fm and, of course, calculations that show that at least some observable is sensitive to the equation of state.

We conclude that at this time the central collisions defined by $b \leqslant 4$ fm still show finite particle effects and disagree with hydrodynamic predictions. Furthermore, the results are not very sensitive to moderate variations of the equation of state. Thus, our attempt to deduce $W(\rho,T)$ seems foiled-at least temporarily.

III.3 Classical Equations of Motion (CEM)

Another demonstration that the single nucleon inclusive spectra are insensitive to specific details of the dynamics comes from the CEM calculations of Bodmer et al.[8.3]. Newton's equations have been integrated for two types of scattering equivalent potentials ($V_1 = V_{st}$ and $V_2 = V_{tr}$ in Fig. 10E) that yield identical asymptotes but differ in the classical trajectory near the distance of closest approach. For dense systems such potentials could in principle lead to different final momentum distributions if asymptotic conditions are not reached between successive collisions.

The constraint on both potentials is to reproduce the experimental average momentum transfer in nucleon-nucleon collisions and σ_{NN}. One potential, V_1, is the sum of a long range attractive and a short range repulsive Yukawa. The second potential V_2 is a momentum dependent, scattering equivalent potential.

For Ne + NaF, the characteristics of the solutions for zero impact parameter collisions are shown in Fig. 10. In the top part of Fig. 10 the average rapidity, $y = 1/2 \ln(1 + V_{\parallel})/(1 - V_{\parallel})$, of the projectile nucleons is shown as a function of time in units of $(E_L/400)$ fm/c. The left hand side is for V_1 and the right side is for V_2. We note first that there are roughly three phases of the reaction for all incident energies. (1) diving $0 < t^* \lesssim 5$ fm/c, (2) compression $5 \lesssim t^* \lesssim 10$ fm/c, (3) expansion $t^* \gtrsim 10$ fm/c. In the diving phase the nuclei are simply interpenetrating. It takes on the order of two mean free paths (~4 fm) for the energy loss to become appreciable. In the compression phase the rate of multiple collisions increases rapidly and the density reaches its maximum value. Rapidly, the incident energy is dissipated in this phase. Finally, between 10-15 fm/c the reaction is essentially over and the system continues to expand without much more redistribution of the momentum distribution. This is seen clearly in Fig. 11 where the invariant single proton inclusive cross section is plotted as a function of time. At $t^* = 5$ fm/c only a small fraction of nucleons have scattered away from the beam direction. However, by $t^* = 10$-15 fm/c the distribution has reached its asymptotic form.

Now compare the results for V_1 and V_2. The maximum compression is appreciably different in Fig. 10 between 5-10 fm/c. Also, we can see appreciable differences at 90° in the cm frame between the momentum distributions at $t^* = 5$ fm/c. However, by 10 fm/c much of the difference in the spectra are lost, and asymptotically no sensitivity to the form of the potential can be seen! Recall that this is for the ideal case $b = 0$.

For impact parameter averaged collisions these calculations agree as well with the data as does the simple statistical model. What we are seeing in Fig. 11 explicitely is the dominance of phase space and geometry and no final sensitivity to the dynamics.

III.4 Billiard Balls

Before getting to the sophisticated cascade codes, it is worth mentioning a very instructive study of nuclear collision made by E. Halbert.[9.10] This study involves playing three dimensional numerical billiards. Both projectile and target are assumed to be a simple collection of billiard balls. The two groups are allowed to collide and the final momentum distribution then analized. The game is clean and no English (Fermi motion, binding, Pauli principle) is given to the balls. For Ne+U the results are shown in Fig. 12. They are quite similar to the hydrodynamic results in Fig. 7. The most interesting aspect of those calculations is a study of the sensitivity of the results to the assumed properties of the billiard balls (hard or soft). Three varieties of balls were considered (1) hard spheres with diameter 0.9 fm, (2) semisoft balls with a hard core of radius .25 fm and (3) soft balls of diameter 0.9 fm. In the last two cases the nucleons are scattered randomly at the distance of closest approach in the soft parts of the balls. Otherwise they scatter as billiard balls.

The dynamical paths in the three cases differs. For example $\rho_{max} = 2,3,3.5$ respectively.[9.1] However, the final spectra are again insensitive to the type of ball played with.[9.3] This gives us the third piece of evidence supporting the hydrodynamic and classical equations of motion results showing that inclusive spectra do not reveal much about the precise dynamical path.

III.5 Intranuclear Cascade Models

The billiard ball model is the prototype of more elaborate intranuclear cascade models[9.2-9.9] that use experimental nucleon-nucleon cross sections. The former has the great virtue of being a clean, classical model, but it clearly neglects several essential physical effects. Three important ones are Fermi motion, binding and Pauli Principle. Of course, all three effects can only be treated rigorously within a quantum theory. However, various classical precriptions have been invented to mock up their effects. In this section we discuss these prescriptions and compare results with data.

The simplest prescription to include Fermi motion is to give each nucleon in the rest frame of either projectile or target an initial momentum $\underset{\sim}{p}$ chosen from a degenerate Fermi gas distribution for a Fermi energy $E_F(r) = (3\pi^2\rho/2)^{2/3}/2m$, where ρ is the nuclear density. This is done in Refs. (9.8,9.9). The problem here is that nuclei simply disintegrate even without a collision. Therefore, the predicted final distributions are always unreliable within a Fermi momentum radius around the projectile and target rapidities. It is hoped that for high energy collisions, the intermediate rapidity and high $p_\perp$ regions however are adequately treated. A more realistic recipe for taking Fermi motion into account is to introduce[9.7] a classical potential $V(r)$ such that $E_F(r) + V(r) = -B$ where $B \approx 8$ MeV is the binding energy of the least bound nucleon. This recipe at least guarantees that the nuclei do not disintegrate before impact. An incident nucleon with lab energy ε rolls down the potential well and acquires a kinetic energy $\varepsilon(r) = \varepsilon - V(r) > \varepsilon$ before it collides with a bound nucleon. After scattering in the well, both nucleons are slowed down as they climb out of the well and even refraction of the momenta is sometimes treated[9.7]. The main assumption is that the mean field $V(r)$ is not influenced by the scattering process. This is reasonable for pA or πA scattering, but for AA scattering the self consistent field could change very much as most of the nucleons scatter out of the potential well. Furthermore, the doubling of the density on interpenetration will change the potential by a about factor of two. An example of the time dependence of the classical potential is given in the EOM calculations of Ref. (8.3). Time

dependent Hartree-Fock calculations also show a large time dependence of the mean field. We conclude that the present prescriptions for Fermi motion and binding in intranuclear cascade models are not very satisfactory for nuclear collisions.

Another questionable prescription is the mocking up of the Pauli Principle by forbidding NN collisions when one of the nucleons would emerge with an energy (in the static well) below some cutoff value (~50 MeV). This restricts greatly the number of soft scatterings and decreases the number of cascade nucleons that emerge from the nuclei.

In Fig. 13, we compare the latest cascade calculations (including cascade-cascade scatterings)[9.7] with the Ne+U data. Relative to the billiard ball model in Fig. 12, the cascade calculation including Fermi motion leads to a much broader quasielastic peak at 30° and somewhat larger yields at backward angles. This is qualitively what we expected. There is however a serious discrepancy at forward angles and low energy. There are more low energy protons in the data than in the calculation. Without the binding and Fermi recipe, the billiard ball calculations however overestimate this low energy proton yield. Results between the billiard ball and cascade calculations have been reported in Ref. (9.5). In that version of cascade only a few of the recipies of Ref. (9.7) were included. Thus, the choice of the recipe seems to lead up to a factor of three differences in the low energy region. We conclude that cascade codes cannot make unambiguous predictions in this region. Of course, with the right choice of prescriptions any data could be fit, but the physical significance of that fit would remain unclear.

For nuclear collisions at energies $\gtrsim$ 1 GeV/nucleon, the cascade calculations reproduce well the high momentum component[15.1,15.2] of the spectra as seen in Fig. 14A,C. However, as we saw in Fig. 4, this kinematic region is dominated by geometry and phase space considerations, so that it is not surprizing that the cascade model fits well in Fig. 14. Indeed, the cascade code of Ref. 9.8-9.9 also fits these particular data well as seen in Fig. 15.

Another comparison of cascade calculations with data is shown in Fig. 16 for the two proton, in-to-out of plane correlation

function C = (coincidence rate of protons at $\theta_{cm} = 90°$, $\phi_1 - \phi_2 = 180°$)/(coincidence rate of protons at $\theta_{cm} = 90°$, $\phi_1 - \phi_2 = 90°$). Both cascade models account for the data. Comparing again to the statistical model results in Fig. (4c), we conclude that the weight, $\sigma_{AB}(1,1)$, of the quasielastic component does indeed follow from simple geometrical considerations as in Eq. (7,8).

An important aspect of intranuclear cascade models is that they offer a theoretical tool to look *inside* nuclear collisions. As we have seen, most observables that we can measure experimentally tell us very little about the high compression phase of the reaction. Unlike colliding plasma beams which we can analyze by stiking a volt meter into the reaction zone, we have not found a clean way of probing the nuclear dynamics during the interesting compression phase that lasts only ~10 fm/c. Intranuclear cascade models can, however, give us detailed snap shots of the collision which may be realistic. In any case, they allow us to test simplified models such as the fireball model.

In Fig. 17, we show several examples of the useful information that can be extracted from cascade codes. These plots were obtained from the cascade calculations of Cugnon et al.[9.9]. The reaction studied was $^{40}Ca + ^{40}Ca$ at zero impact parameter for various beam energies. We see in Fig. 17A that between 0.4 and 3 GeV/nucleon the maximum density is significantly larger than the trivial interpenetration value $2\gamma\rho_o$. Note that the triangles show what happens if Δ production were ignored. Pion productions leads to significantly higher densities. This is also reflected in Fig. 17D that shows $Y(t) = \langle p_\perp^2 \rangle / \langle p_\parallel^2 \rangle$ in the cm frame as a function of time. Y(t) measures the degree of thermalization achieved. In thermal equilibrium $Y_{eq} = 2$. In part (a) of Fig. 17D the final $Y_{final} = Y(\infty)$ is plotted vs. beam energy. Note that above 1 GeV/nucleon, $Y(\infty)$ is significantly less than the equilibrium value. Also from the triangles we see how much pions help in converting parallel momentum into random motion. The incomplete thermalization even for this zero impact parameter collision is also seen in Fig. 17B. For each beam energy the rapidity distribution dN/dy and the $p_\perp$ distribution $dN/dp_\perp$ are shown. The dashed lines are attempts to fit the histogram with a Boltzmann distribution. The "temperature" from the fit is indicated. Note that $T_\parallel > T_\perp$ in

accordance with Fig. 17D. Thus we cannot speak of a single fireball. Rather there is incomplete thermalization due to finite mean free path effects. The firestreak model is also ruled out because for b=0 that would give $T_{\parallel} = T_{\perp}$. In Fig. 17Db, we can see the time history of equilibration. As in Fig. 10A (note different definition of Y there) there appears to be the same three qualitative phases of the collision: diving, compression, expansion. The dashed curve shows the luminocity L = number of binary collisions per unit time. As the nuclei dive into each other L(t) increases linearly as the number of participants increases. By 5 fm/c a rapid transfer of parallel momentum to perpendicular momentum takes place as the luminocity reaches its maximum value $L_{max} \sim A_p \rho_T \sigma_{NN} c \sim 24\ (\mathrm{fm/c})^{-1}$. Then, however, rapid expansion takes place, $\rho(t)$ decreases, and around 10 fm/c the sudden decrease of L(t) signals the end of the redistribution and randomization of momenta. Because of this expansion Y(t) only reaches 1/2 of the equilibrium value. If only the collision lasted another 5 fm/c, equilibrium may have been reached. $^{40}Ca + {}^{40}Ca$ is simply too small a system to reach equilibrium. On the other hand, for U + U the interaction time should be $(238/40)^{1/3} \approx 1.8$ times longer. In that case, b = 0 U + U collisions have a much better chance of reaching equilibrium.

III.6 Models of Pion Production

For beam energies $\gtrsim 1$ GeV/nucleon, the average number of pions produced per participant nucleon is observed[15,6] to increase linearly with the beam energy per nucleon E_L as $n_\pi/A \approx 0.15\ (E_L/1\ \mathrm{GeV})$. Furthermore, the pion multiplicity distribution is observed[15,6] to be of Poisson form for fixed participant number, indicating that pions are produced and absorbed one at a time[16]. The main mechanism for producing pions in nucleon-nucleon scattering in this energy range is through $NN \to N\Delta$, where Δ is the 3,3 resonance at 1236 MeV with a width $\Gamma_\Delta \sim 110$ MeV. It is therefore reasonable to assume that in nuclear collisions pions are produced incoherently through the same mechanism. We note that pion condensation instabilities could lead to coherent pion production, but a recent estimate[4] suggests that only a small fraction of the observed pions could be coherently produced.

While all intranuclear cascade codes treat pion production through $NN \to N\Delta$, there are different prescriptions to handle pion absorbtion. The simplest one is to ignore the decay of the Δ but allow $N\Delta \to NN$. This is the $\Gamma_\Delta = 0$ prescription used by Cugnon et al.[9.8]. The resulting average pion multiplicity comes out correctly but the spectral shapes (see Fig. 15B) do not agree with data. The calculations lead to too few low energy pions and too many high energy pions. This simply reflects that pions produced via $\Delta \to \pi N$ emerge with ~200 MeV/c momentum in the Δ rest frame. The data[15.1,15.2] show, on the other hand, the the spectrum of pions is much more thermalized. Thus, the assumption that Δ's do not decay until the end of the collision is not supported by data.

In the version by Yariv and Fraenkel[9.7], $\Delta \leftrightarrow \pi N$ is allowed as well as $N\Delta \leftrightarrow NN$. Thus within 2 fm/c after creation, a Δ can decay to πN. The π's can then scatter elastically $\pi N \to \pi N$ via free space cross sections and be absorbed via $\pi NN \to N\Delta \to NN$. Results[9.7] with such a cascade are shown in Fig. 14B,C. Now the spectral shapes come out well but the normalization is too high. In this calculations interactions between cascade particles were ignored. Including these additional interactions in the latest calculations leads to more pion absorbtion and better agreement with the data as shown in Fig. 18. The consistency of these prescriptions with pA and πA data have also been verified recently[9.7]. Thus, the gross features of the pion spectra can be understood in this way.

There are however, fine details of the pion spectra (at the level of $\lesssim$ 30%) that are not adequately treated via such cascade calculations. In particular, it has become apparent that Coulomb effects can lead to unusual distortions in certain kinematical domains. See References 17 for details. At this time the precise way in which Coulomb effects, nuclear shadowing, and Δ production conspire to produce such details in under lively debate.

The final topic that I will discuss here as pion interferometry[18]: the study of correlation of two identical pions with small relative momenta $\underset{\sim}{q} = \underset{\sim}{p}_1 - \underset{\sim}{p}_2$. This is one of the few topics in nuclear collisions where quantum mechanics is crucial. Recall the discussion in section II.2 where one of the criteria

for the validity of classical mechanics was $qR \gg \hbar$. To see quantum effects we must look for small momentum differences $q \lesssim \hbar/R \approx 50$ MeV/c. For such relative momenta the Bose nature of identical pions becomes important and leads to interference patterns known in optics as the Hanbury-Brown and Twiss effect[18]. From the correlation function it is possible to extract geometrical information on the interaction region where the pions were produced. However, an additional property of the correlation function $R(\underset{\sim}{p}_1,\underset{\sim}{p}_2)$ = (coincidence rate of identical pions with relative momentum q)/(random rate from different events) is that if a fraction of the pions $D(\underset{\sim}{p})$ of momentum $\underset{\sim}{p}$ are produced coherently, then the intercept of R at $\underset{\sim}{p}_1 = \underset{\sim}{p}_2 = \underset{\sim}{p}$ would be[18.3] $1-D^2(\underset{\sim}{p})$. $D(\underset{\sim}{p})$ is the degree of coherence of the pion field. Coulomb final state interactions modify this simple relation in a definite way. For completely chaotic pion fields (D=0), R has the form[18.3]

$$R(\underset{\sim}{p}_1,\underset{\sim}{p}_2) = G(\underset{\sim}{p}_1'-\underset{\sim}{p}_2')(1 + |\rho(\underset{\sim}{p}_1'-\underset{\sim}{p}_2')|^2) \tag{18}$$

where G(q) is the Coulomb Gamow factor and ρ is the Fourier transform of the space-time region where the pions were produced. The momenta $\underset{\sim}{p}_i'$ Eq. (18) are shifted relative to the observed $\underset{\sim}{p}_i$ due to the interaction of the pions with the nuclear Coulomb field as discussed in Ref. (17.5).

The very preliminary data of Zajc et al.[18.5] on pion interferometry is shown in Fig. 19. The dashed curve is obtained via Eq. (18) assuming a 5 fm radius pion source. The agreement with the data excludes a degree of coherence larger than ~ 20% and is consistent with a completely chaotic pion field. This result thus adds further support to the basic assumption in cascade models that pions are produced incoherently in nuclear collisions.

IV. SUMMARY AND OUTLOOK

The purpose of this report has been to provide an up to date introduction to the models of relativistic nuclear collisions. Clearly many topics and models have been omitted. Particular attention was paid to the question of what we can learn about dense,

highly excited nuclear matter from inclusive data. The second generation of experiments[1] have provided us a large variety of data on both one particle and two particle inclusive cross sections, often triggered on more central collisions. Where do we stand?

We have learned a tremendous amount about the basic reaction mechanism. The role of geometry, phase space, and kinematics has been shown to dominate much of the gross features of the data. However, initial state interactions (Fermi motion) and final state interactions (composite production, Coulomb fields, and nuclear shadowing) often lead to complicated distortions of the particle spectra. We have learned that finite mean free path effects cannot be ignored in any reaction studied so far. The spectra show clear non-equilibrium effects, and with the two proton correlation experiments[15.1] direct proof of the existence of the quasi-elastic, $\sigma(1,1)$, component has been found.

The sifnificant non-equilibrium component even in near central Ne + U collisions virtually rules out a 1-fluid hydrodynamic description of such data. This was one of our initial worries. Since hydrodynamics is the only direct link between data and the nuclear equation of state $W(\rho,T)$, the prospects of determining W from data do not seem promising. The problem is not that we are looking at the wrong observables (central triggered proton inclusive cross sections), but that hydrodynamics does not take into account finite mean free paths and binding that seem essential from the data.

On the other hand, we saw that the high momentum components of inclusive spectra[15.1] are very insensitive to dynamical details of the compression phase. Thus, we cannot hope to learn about high density nuclear matter from such data either.

Pion production above 1 GeV/nucleon is important, but again simple incoherent $NN \rightarrow N\Delta$ reactions seem to account for the gross features of the pion spectra as long as π absorbtion and rescattering are treated in a consistent manner.

It must be emphasized though that we do not have a complete understanding of the reaction mechanism. Many detailed features of the data such as the π^+ bump[15.7] at $y = y_{cm}$, $p_\perp \approx 0.5\ m_\pi$ are only partially understood. The low energy $E < 50$ MeV, $Ne + U \rightarrow p$ data are also not well understood. In these cases, we still have

to sort out the complex interplay of the many elements of the reaction mechanism.

While reaction mechanism studies will continue in the near future, what new directions of research can be pursued? The third generation of experiments (see Gutbrod[1]) will concentrate on more exclusive analysis of nuclear collisions. In particular, jet analysis of the final fragments will provide useful information on the net momentum transfer two nuclei impact to one another at these energies. In some sense, this is a continuation of deep inelastic studies from low energy nuclear collisions. At high energies the nuclei disintegrate upon impact, but through jet analysis the bulk momentum transfer can be analyzed. Sphericity studies will also enable us to define a reaction plane. This will help untangle nuclear shadowing and Coulomb effects for instance.

Another interesting line of research to continue is the projectile fragmentation studies (see Schroeder[1]). Already many neutron rich nuclei have been discovered in such experiments, and the possibility to do nuclear structure studies on nuclei near the neutron drip line seems promising. In addition, there is increased hope at present that projectile fragments with momentum far exceeding the beam momentum and target fragments in the backward hemisphere can probe the high momentum component of nuclear wavefunctions.[10]

As to novel states of nuclear matter, the only tantalyzing carrot we have at the moment are the anomalous short mean free paths reported[9] for secondary fragments in emulsions. It appears that a small fraction ~6% of the projectile fragments in peripheral nuclear collision exhibit an unusually large (~10X geometrical) reaction cross section. Such fragments seem to defy conventional nuclear physics explanation at present. If true, it would be ironical if we got bogged down cutting weeds in violent central collisions searching for new states of matter when gentle peripheral collisions have been holding out the flowers all along.

ACKNOWLEDGEMENTS:

The analysis in this report arose out of numerous private discussions. I am particularly grateful to J. Knoll, R. Nix, A. Bodmer, E. Halbert, J. Cugnon, Z. Fraenkel, H. Gutbrod, R. Stock, S. Nagamiya, W. Zajc, and G. Westfall for making available their unpublished results and ideas. Valuable conversations with S. Koonin, J. Randrup, H. Stöcker, A. Sandoval, K. Wolf, and S. K. Kauffmann are also gratefully acknowledged.

This work was supported by the Office of Nuclear Physics of the U.S. Department of Energy under contract W-7405-ENG-48.

References

1. For reviews of current data, see talks of H.Gutbrod and L.Schroeder elsewhere in these Proceedings.
2. M.Gyulassy, LBL-6594, in Fyzika (Yugoslavia) 9, Suppl. 4 (1977), p.623.
3. Recent reviews and conferences:
   - 3.1 A.Goldhaber, H.Heckman, Ann. Rev. Nucl. Part. Sci. 28 (1978) 161;
   - 3.2 J.R.Nix, Prog. Part. Nucl. Phys. 2 (1979) 237;
   - 3.3 Proc. Topical Conf. on Heavy Ion Collisions, Fall Creek Falls, ORNL Report Conf-770602 (1977);
   - 3.4 Proc. of Symposium on Relativistic Heavy Ion Research, March 1978, GSI-Darmstadt;
   - 3.5 Fourth High Energy Heavy Ion Summer Study, LBL-7766, Conf-780766, July 1978.
4. M.Gyulassy, "Pion condensation and instabilities: current theory and experiment," LBL-10883, July 1980, Proc. of the Joint NSF-Japan Seminar on High Energy Nuclear Reactions, Hakone, Japan.
5. Pion condensates, abnormal nuclear matter:
   - 5.1 A.B.Migdal, Rev. Mod. Phys. 50 (1978) 107;
   - 5.2 W.Weise, G.E.Brown, Phys. Reports 27C (1976) 1;
   - 5.3 T.D.Lee, Rev. Mod. Phys. 47 (1975) 267;
   - 5.4 G.Baym, D.K.Campbell, H.Pirner, Les Houches 1977 Lectures, Session XXX, Vol. 2.
6. J.I.Kapusta, Nucl. Phys. B148 (1979) 461 and references therein; O.K.Kalashnikov and V.V.Klimov, Phys. Lett. 88B (1979) 328.
7. J.D.Walecka, Ann. Phys. 83 (1974) 491.
8. References for classical equation of motion method:
   - 8.1 A.R.Bodmer, C.N.Panos, Phys. Rev. C15 (1977) 1342;
   - 8.2 A.R.Bodmer, p.309 of Ref. 3.3, p.347 of Ref. 3.4;
   - 8.3 A.R.Bodmer, C.N.Panos, A.D.MacKellar, Argonne preprint;
   - 8.4 L.Wilets, E.M.Henley, M.Kraft, A.D.MacKellar, Nucl. Phys. A282 (1977) 361.
   - 8.5 L.Wilets, Y.Yariv, R.Chestnut, Nucl. Phys. A301 (1978) 359;
   - 8.6 D.J.E.Callaway, L.Wilets, Y.Yariv, Nucl. Phys. A327 (1979) 250;

8.7 M.Sano et al., J. Phys. Soc. Japan 44, Suppl. (1978).

9. Intranuclear Cascade models:

9.1 J.P.Bondorf, H.T.Feldmeier, S.Garpman, E.C.Halbert, Phys. Lett. 65B (1976) 217; Z. Phys. 279 (1976) 385;

9.2 R.K.Smith, M.Danos, p.363 of Ref. 3.3;

9.3 K.K.Gudima, V.D.Toneev, Yad. Fiz. 27 (1978) 658 [Sov. J. Nucl. Phys. 27 (1978) 351];

9.4 K.K.Gudima, H.Iwe, V.D.Toneev, J. Phys. G5 (1978) 229;

9.5 J.D.Stevenson, Phys. Rev. Lett. 41 (1978) 1702;

9.6 W.Jaisli, H.Kuhlmann, C.C.Noack, p.365 of Ref. 3.4;

9.7 Y.Yariv, Z.Fraenkel, Phys. Rev. C20 (1979) 2227; and to be published.

9.8 J.Cugnon, "A Monte-Carlo calculation of high energy heavy ion interactions," Cal Tech preprint MAP-9, January 1980.

9.9 J.Cugnon, T.Mizutani, J.Van Der Meullen, "Equilibration in relativistic nuclear collisions: a Monte Carlo calculation," Cal Tech preprint MAP-10, February 1980.

9.10 E. C. Halbert, "Density patterns and energy-angle distributions from a simple cascade scheme for fast Ne + U collisions," ORNL preprint (1980).

10. Hard scattering models:

10.1 S.E.Koonin, Phys. Rev. Lett. 39 (1977) 680;

10.2 R.L.Hatch, S.E.Koonin, Phys. Lett. 81B (1979) 1;

10.3 I.A.Schmidt, R.Blankenbecler, Phys. Rev. D15 (1977) 3321;

10.4 R.H.Landau, M.Gyulassy, Phys. Rev. C19 (1979) 149;

10.5 M.Chemtob, Nucl. Phys. A314 (1979) 387.

11. Hydrodynamic models:

11.1 A.A.Amsden, G.F.Bertsch, F.H.Harlow, J.R.Nix, Phys. Rev. Lett. 35 (1975) 905;

11.2 A.A.Amsden, F.H.Harlow, J.R.Nix, Phys. Rev. C15 (1977) 2059;

11.3 A.A.Amsden, A.S.Goldhaber, F.H.Harlow, J.R.Nix, Phys. Rev. C17 (1978) 2080;

11.4 A.A.Amsden, J.N.Ginocchio, F.H.Harlow, J.R.Nix, M.Danos, E.C.Halbert, R.K.Smith, Phys. Rev. Lett. 38 (1977) 1055;

11.5 G.Bertsch, A.Amsden, Phys. Rev. C18 (1978) 1293;

11.6 a) J.R.Nix, D.Strottmann, Preprint LA-UR-80-814, March 1980.

b) J.R.Nix, D.Strottmann, A.Sierk, Preprint LA-UR-80-, April 1980.

11.7 Y.Kitazoe,et al.,Prog. Theor. Phys. 56 (1976) 860.

11.8 W.Scheid, H.Müller, W.Greiner, Phys. Rev. Lett. 32 (1974) 741.

11.9 H.Stöcker, J.A.Maruhn, W.Greiner, Phys. Lett. 81B (1979) 303; Z. Physik A290 (1979) 297.

11.10 H.Stöcker, R.Y.Cusson, J.A.Maruhn, W.Greiner, Z. Phys. A294 (1980) 1.

11.11 H.Stöcker, J.A.Maruhn, W.Greiner, Z. Phys. A293 (1979) 173.

11.12 C.Y.Wong, J.A.Maruhn, T.A.Welton, Nucl. Phys. A253 (1975) 469, Phys. Lett. 66B (1977) 19.

11.13 J.A.Maruhn, Ref. 3.3.

11.14 H.H.K.Tang, C.Y.Wong, Phys. Rev. C21 (1980) 1846.

11.15 P.Danielewicz, Nucl. Phys. A314 (1979) 465.

11.16 L.P.Csernai, B.Lukács, "Viscous hydrodynamical model for relativistic heavy ion reactions," preprint KFKI-1979-58, Hungary, 1979.

11.17 L.P.Csernai, G.Fai, "Simple models for almost central asymmetric heavy ion collisions at moderate energies," Preprint KFKI-1979-66, Hungary, 1979.

11.18 P.J.Siemens, J.O.Rasmussen, Phys. Rev. Lett. 42 (1979) 880.

12. Transport models:

12.1 J.Hüfner, J.Knoll, Nucl. Phys. A290 (1977) 460.

12.2 J.Knoll, J.Randrup, Nucl. Phys. A324 (1979) 445; and to be published.

12.3 H.J.Pirner, B.Schurman, Nucl. Phys. A316 (1979) 461.

12.4 B.Schurman, Phys. Rev. C20 (1979) 1607.

12.5 J.Randrup, Nucl. Phys. A316 (1979) 509.

12.6 P.Hecking, H.Pirner, Nucl. Phys. A333 (1980) 514.

12.7 R.Malfliet, Phys. Rev. Lett. 44 (1980) 864.

13. Thermal and phase space models:

13.1 G.D.Westfall, J.Gosset, P.J.Johansen, A.M.Poskanzer, W.G.Meyer, H.H.Gutbrod, A.Sandoval, R.Stock, Phys. Rev. Lett. 37 (1976) 1202.

13.2 W.D.Myers, Nucl. Phys. A296 (1978) 177.

13.3 J.Gosset, J.I.Kapusta, G.D.Westfall, Phys. Rev. C18 (1978) 844.

13.4 S.Das Gupta, Phys. Rev. Lett. 41 (1978) 1450.

13.5 J.Knoll, Phys. Rev. C20 (1979) 773.

13.6 J.Knoll, "Do we see finite particle number effects in central high energy heavy ion collisions," Preprint Max-Planck-Institut, MPI H-1979-V37.

13.7 S.Bohrmann, J.Knoll, "Finite particle number effects in high energy nuclear collisions: implications on pion spectra," preprint LBL-10970 (1980).

13.8 E.Fermi, Prog. Theor. Phys. 5 (1950) 570.

14. Models for composite production:

14.1 H.H.Gutbrod, A.Sandoval, P.J.Johansen, A.M.Poskanzer, J.Gosset, W.G.Meyer, G.D.Westfall, R. Stock, Phys. Rev. C16 (1977) 629.

14.2 A.Mekjian, Phys. Rev. Lett. 38 (1977) 640; Phys. Rev. C17 (1978) 1051; Nucl. Phys. A312 (1978) 491; Phys. Lett. 89B (1980) 177.

14.3 S.Das Gupta, Phys. Rev. C18 (1978) 2773.

14.4 J. I. Kapusta, "Mechanisms for deuteron production in relativistic nuclear collisions," preprint LBL-9251.

14.5 I.Montvay, J.Zimányi, Nucl. Phys. A316 (1979) 490.

14.6 C.Noack, M.Gyulassy, S.K.Kauffman, "Test of Square Law for Deuteron Production in Relativistic Nuclear Collisions", Preprint LBL-11053, July (1980).

15. Data references used for figures:

15.1 S. Nagamiya et al., Phys. Lett. 81B (1979) 147.

15.2 S.Nagamiya, "Heavy ion collisions at relativistic energies," LBL-9494 (1979), Proceedings on Heavy Ion Physics, Brookhaven National Laboratory, July 1979.

15.3 R.Stock, et al., Phys. Rev. Lett. 44 (1980) 1243.

15.4 A.Sandoval, et al., Phys. Rev. C21 (1980) 1321.

15.5 H.H.Gutbrod, "Search for Extreme States in Nuclear Matter", Preprint LBL-10624, March 1980.

15.6 A.Sandoval, et al., "Energy Dependence of Multipion Production in High Energy Nucleus Nucleus Collisions", Preprint LBL-10830 (1980).

15.7 K. L. Wolf et al., Phys. Rev. Lett. 42 (1979) 1448.

16. Pion Multiplicity Distribution Models

16.1 M.Gyulassy, S.K.Kauffmann, Phys. Rev. Lett. 40 (1978) 298; S.K.Kauffmann, M. Gyulassy, J. Phys. A11 (1978) 1715.

16.2 J.Vary, Phys. Rev. Lett. 40 (1978) 294.

16.3 J.Knoll, et al., Nucl. Phys. A308 (1978) 500.

16.4 Y.Afek, et al., Phys. Rev. Lett. 41 (1978) 849.

17. Coulomb Final State Interactions

17.1 W. Benenson, et al., Phys. Rev. Lett. 44 (1980) 54.

17.2 G. Bertsch, Nature 283 (1980) 280.

17.3 K.G. Libbrecht, S.E.Koonin, Phys. Rev. Lett. 43 (1979) 1581.

17.4 J.Chiba et al., Phys. Rev. C20 (1979) 1332; K.Nakai et al., Phys. Rev. C20 (1979) 2210.

17.5 M.Gyulassy, S.K.Kauffmann, "Coulomb Effects in Relativistic Nuclear Collisions", Preprint LBL-10279, March 1980.

18. Pion Interferometry of Nuclear Collisions.

18.1 M.Gyulassy, Ref. (3.4) p. 273.

18.2 F.B.Yano, S.E.Koonin, Phys. Lett. 78B (1978) 556.

18.3 M.Gyulassy, S.K.Kauffmann, L.W.Wilson, Phys. Rev. C20 (1979) 2267.

18.4 S.Y.Fung, et al., Phys. Rev. Lett. 41 (1978) 1592.

18.5 W.Zajc, et al. Bull. Am. Phys. Soc. (April 1980), and to be published.

19. Juicy carrot:

E.M.Friedlander, R.W.Gimpel, H.H.Heckman, Y.J.Karant, B.Judek, E.Ganssauge, "Evidence for Anomalous Nuclei among Relativistic Projectile Fragments from Heavy Ion Collisions at Bevalac Energies", Preprint LBL-11136 (1980).

Figure Captions:

Fig. 1. Hierarchy of theoretical frameworks for relativistic nuclear collisions.

Fig. 2. Geometry of fireball (a) and (b) firestreak models.

Fig. 3. a) Finite number phase space distribution, Eq. (13), $\phi_{mn} = F_{m,n}(\varepsilon_{cm})/(m+n)$, from Ref. 13.6.
b) Proton spectra at 90° cm with $B = 1$ (inclusive) and $B = \delta^2(\underset{\sim}{b})$ (high multiplicity) in Eq. (7). Data are from Ref. 15.1. Solid curves are statistical model predictions with Fermi momentum averaging.[13.6] Dashed line is thermal model prediction (using Eq. (14)).

Fig. 4. a) Proton inclusive spectra[15.1] and statistical model predictions.[13.5]
b) Proton angular distributions viewed from the c.m. frame. Three proton c.m. energies are considered. Both inclusive and high multiplicity selected data are shown. The corresponding statistical model predictions[13.6] solid and dashed respectively are also shown.
c) Coincidence rate of two protons at same lab angle $\theta_i = 40°$ but different azimuthal angles ϕ_i. The ratio plotted is the coincidence rate in plane ($\phi_1 - \phi_2 = 180°$) to the coincidence rate out of plane ($\phi_1 - \phi_2 = 90°$). Data are from Ref. 15.1. Solid curves are as in (b). Dashed curve excluded the knock-out contribution $m = n = 1$ in Eq. (9). Most recent data for C + Pb in Ref. 14.2 indicate a ratio closer to 0.9 than 1.0.

Fig. 5. a) Density contours from viscous hydrodynamical calculations of Stöcker, et al.[11.9-11.11] for various impact parameters as a function of time.
b) $d^2\sigma/dEd\Omega$ for various impact parameters in the same model.

Fig. 6. Three examples of the nuclear matter equation of state, $W_o(\rho)$, Eq. (16), used in hydrodynamical calculations in Ref. 11.6.

Fig. 7. Comparison of charge inclusive data[15.4] (dots) with one fluid hydrodynamical calculations[11.6] (histogram). The results with the three equations of state in Fig. 6 are displayed. Note the insensitivity to the assumed equation of state.

Fig. 8. Comparison of central triggered inclusive proton (x) and charge (dot) data[15.3] with one fluid hydrodynamic calculations. The charge inclusive data include preliminary deuteron and triton spectra.[15.5] Again results with the three equations of state are shown.

Fig. 9. The average associated multiplity ⟨M⟩ for tag counter array of Gutbrod, et al. Ref. (15.3-15.5) as a function of impact parameter b. The error bars indicate variance of distribution for fixed b. These results are obtained via the intranuclear cascade program of Yariv and Fraenkel.[9.7]

Fig. 10. Characteristics of classical equations of motion calculations[9.3] for central (b=0) Ne+NaF collisions at various energies. Left hand plots are for potential $V_1 = V_{st}$ and right hand plots are for $V_2 = V_{tr}$. (A),(B) the average rapidity of projectile fragments and (C), (D) the average central density are plotted against the reduced time t^* in units of (E_L/400 MeV) fm/c. (E) example of scattering equivalent classical trajectory for the two potentials.

Fig. 11. The Lorentz invariant proton cross section in the cm frame in plotted for three times t^* for $b = 0$, Ne+NaF at 800 MeV/nucleon. Again compare the right and left sides for the two scattering equivalent potentials.

Fig. 12. Comparison of billiard ball calculations[9.3] with charged inclusive data[15.4] for Ne+U at 393 MeV/nucleon. The energy units are ENU = 1.63 MeV.

Fig. 13. (A) Preliminary cascade calculations of Yariv and Fraenkel[9.7] including cascade-cascade scattering (histogram) compared with charge inclusive spectra[15.4] for Ne+U at 393 MeV/nucleon .
(B) Percentage of p,d,t,... for same reaction at 90° vs lab energy. Lower plot shows data of Ref. (15.4). Upper plot show firestreak predictions of G. Westfall (unpublished). Right hand scale is for protons.

Fig. 14. Invariant proton and pion inclusive cross sections calculated with the cascade code of Yariv and Fraenkel[9.7] *not* including cascade-cascade interactions. The data are from Nagamiya et al., Ref. (15.1,15.2).

Fig. 15. As in Fig. 14 but now showing calculations (histogram) with the cascade code of Cugnon et al. Ref. (9.8,9.9).

Fig. 16. In-to-out of plane two proton correlation function for $\theta_1^{cm} = \theta_2^{cm} = 90°$ and $\phi_1-\phi_2 = 180°/\phi_1-\phi_2 = 90°$. Data (dots) are from Ref. (15.1,15.2). Left graph shows Cugnon et al predictions (with error bars). Right graph shows Yariv and Fraenkel's preliminary results; dashed curve is with code not including cascade-cascade interactions.

Fig. 17. Cascade calculations of Ref. (9.9) for $b = 0$, Ca + Ca collisions, (A) The maximum density ρ_{max}/ρ_o vs. beam energy is shown for different reaction mechanisms. Triangles are results ignoring pion production. (B) The rapidity distribution $N(y) = d\sigma/dy$ and the perpendicular momentum distribution $N(p_\perp) = d\sigma/dp_\perp$ are shown for bombarding energies 0.4-3 GeV/nucleon. The parallel and perpendicular temperatures are determined by fits to Boltzmann distributions (dashed). (C) Effective proton and pion slope parameters T vs E_{beam}.
(D) $Y(t) = \langle p_\perp^2 \rangle / \langle p_\parallel^2 \rangle$ solid curve (left scale), $L(t)$ = luminocity = number of binary collision per unit time, vs. time. $Y = 2$ in thermal equilibrium.

Fig. 18. π^+ data (dots)[15.7] and cascade calculations[9.7]. Dashed histogram neglects cascade-cascade interactions, solid histogram includes them.

Fig. 19. *Preliminary* data[18.5] on pion interferometry of Ar + KCl at 1.8 GeV/nucleon. R(q) is the coincidence rate for observing a $\pi^-\pi^-$ pair with relative momentum q divided by the random rate from different events. Solid curve shows R(q) for a chaotic field originating from a 5 fm static source. Dashed curve includes Coulomb Gamow factor.

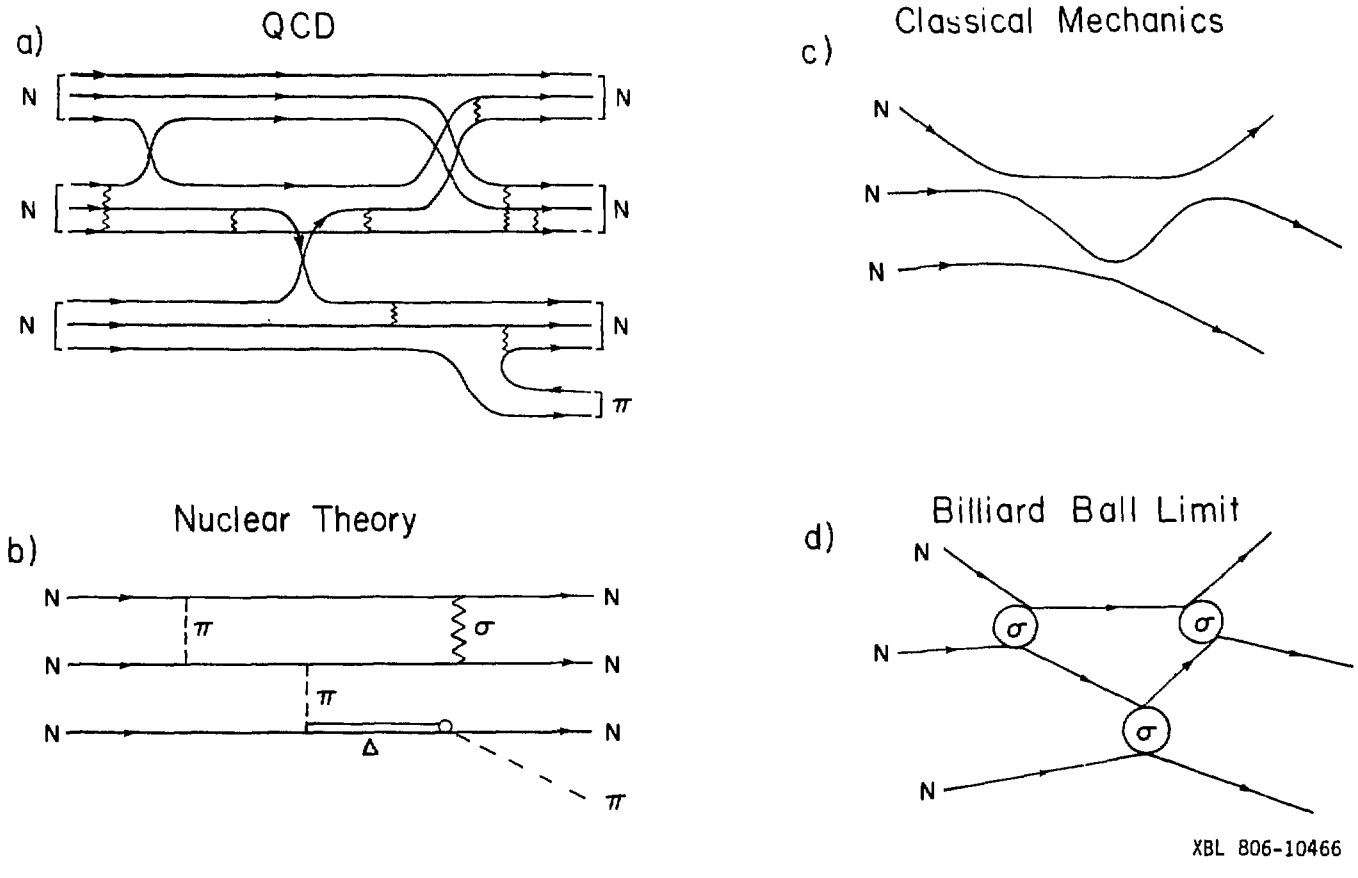
a)
QCD
N
N
N
N
N
N
π
b)
Nuclear Theory
N
N
N
N
N
N
π
π
σ
Δ
π
c)
Classical Mechanics
N
N
N
d)
Billiard Ball Limit
N
N
N
σ
σ
σ
XBL 806-10466

Fig.1

a) Fireball:

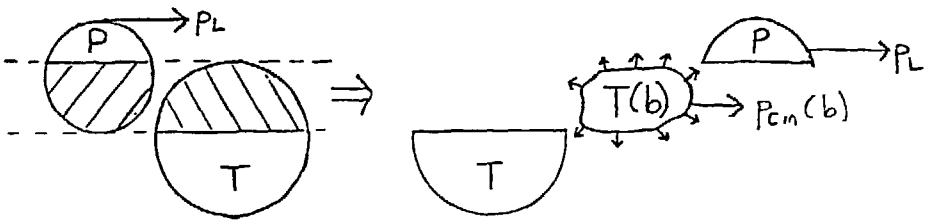

b) Firestream:

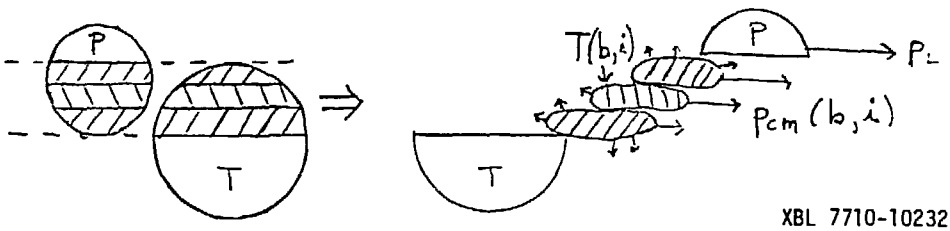

XBL 7710-10232

Fig.2

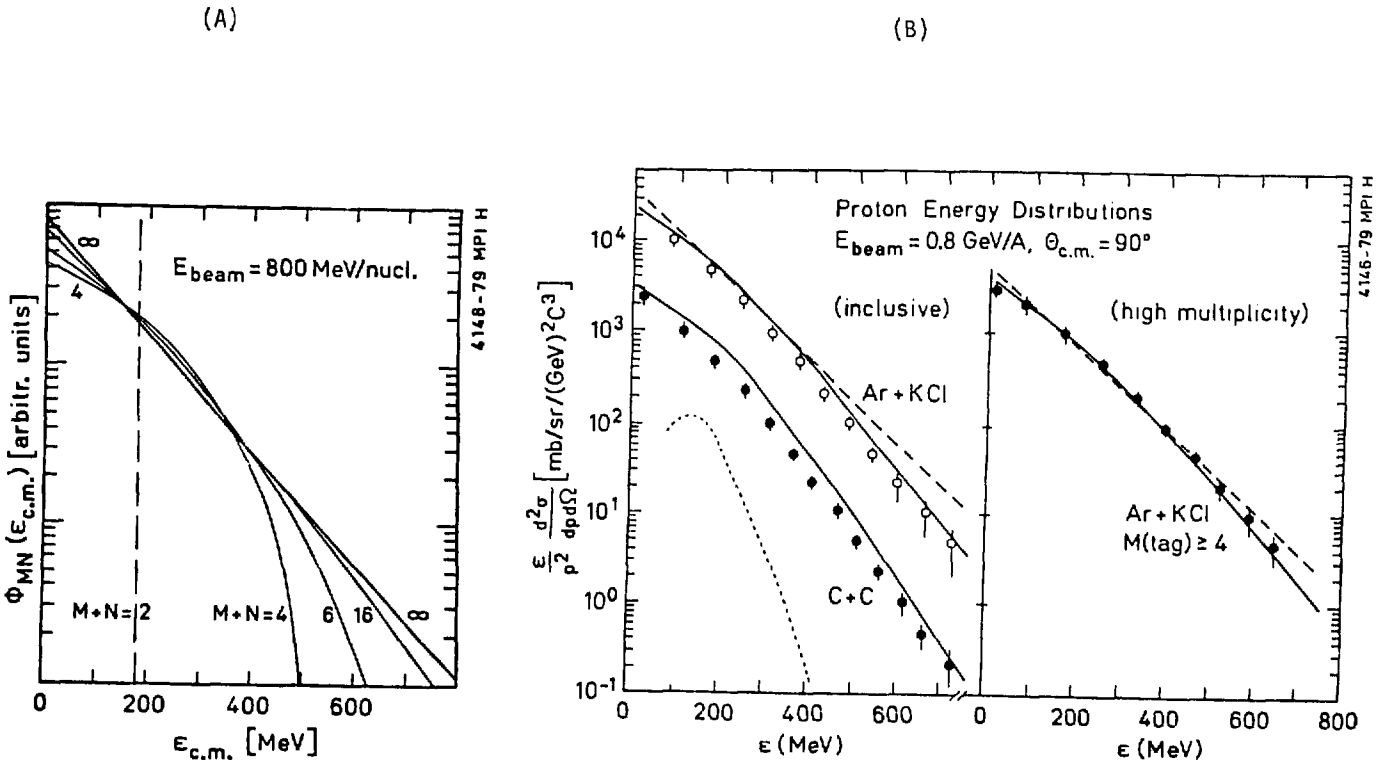
(A)
(B)
E_{beam} = 800 MeV/nucl.
$\Phi_{MN}(\varepsilon_{c.m.})$ [arbitr. units]
M+N=2
M+N=4
6
16
∞
4
$\varepsilon_{c.m.}$ [MeV]
4148-79 MPI H
Proton Energy Distributions
E_{beam} = 0.8 GeV/A, $\Theta_{c.m.}$ = 90°
(inclusive)
(high multiplicity)
Ar + KCl
C + C
Ar + KCl
M(tag) ≥ 4
$\frac{\varepsilon}{p^2}\frac{d^2\sigma}{dp d\Omega}$ [mb/sr/(GeV)^{2}c^3]
ε (MeV)
4146-79 MPI H
XBL 806-10465

Fig. 3

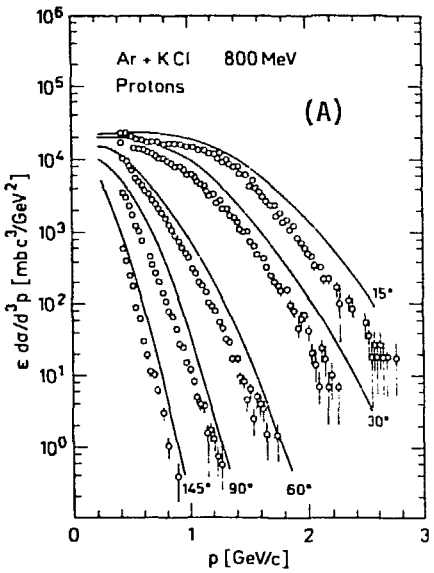
Ar + KCl 800 MeV
Protons
(A)
15°
30°
60°
90°
145°
ε dσ/d³p [mb c³/GeV²]
p [GeV/c]

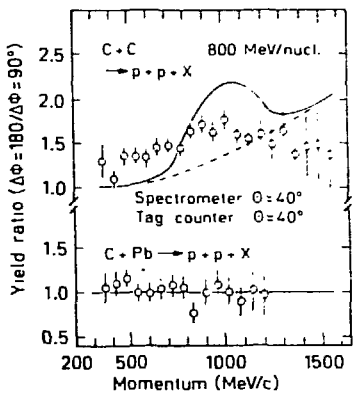
C + C 800 MeV/nucl.
→ p + p + X
Spectrometer Θ = 40°
Tag counter Θ = 40°
C + Pb → p + p + X
Yield ratio (ΔΦ=180/ΔΦ=90°)
Momentum (MeV/c)
(C)

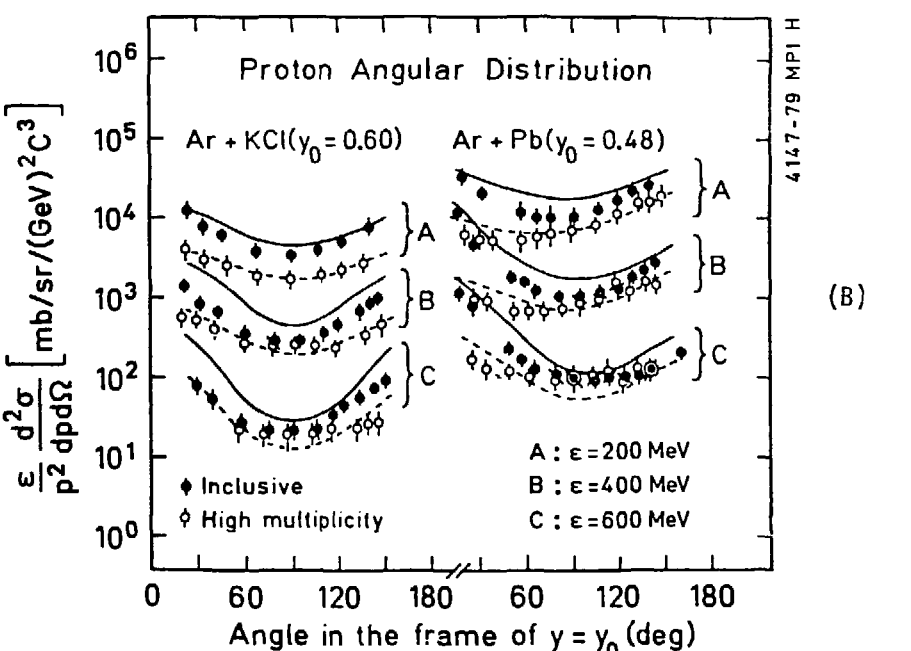
Proton Angular Distribution
Ar + KCl(y0 = 0.60)
Ar + Pb(y0 = 0.48)
4147-79 MPI H
A
B
C
Inclusive
High multiplicity
A : ε = 200 MeV
B : ε = 400 MeV
C : ε = 600 MeV
ε d²σ / p² dpdΩ [mb/sr/(GeV)²c³]
Angle in the frame of y = y0 (deg)
(B)
XBL 806-10464

Fig.4

(A)

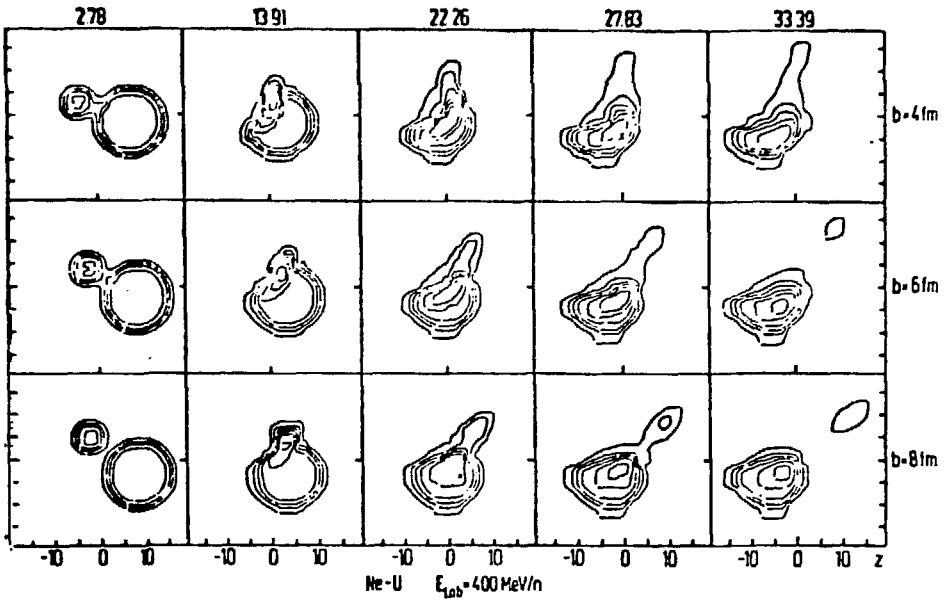

(B)

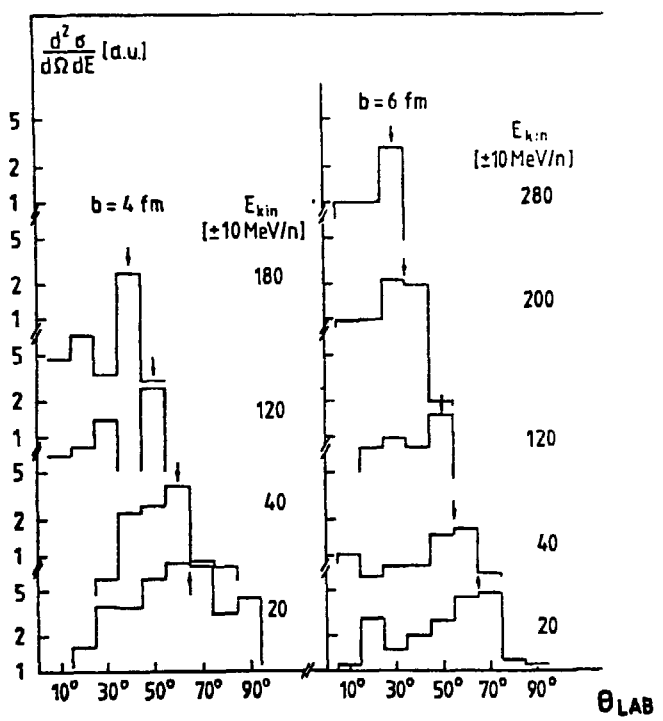

XBL 806-10463

Fig.5

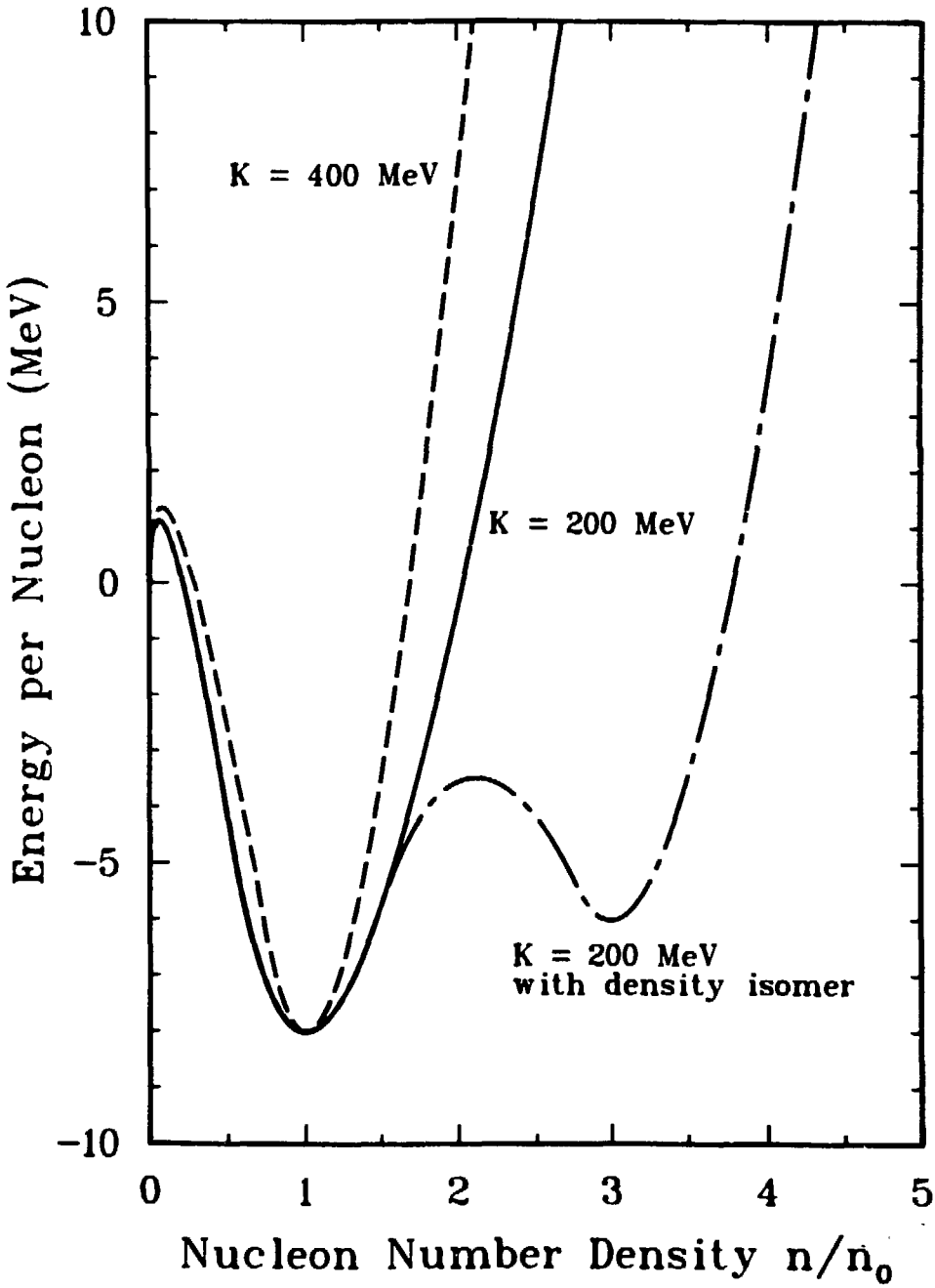

XBL 806-10462

Fig. 6

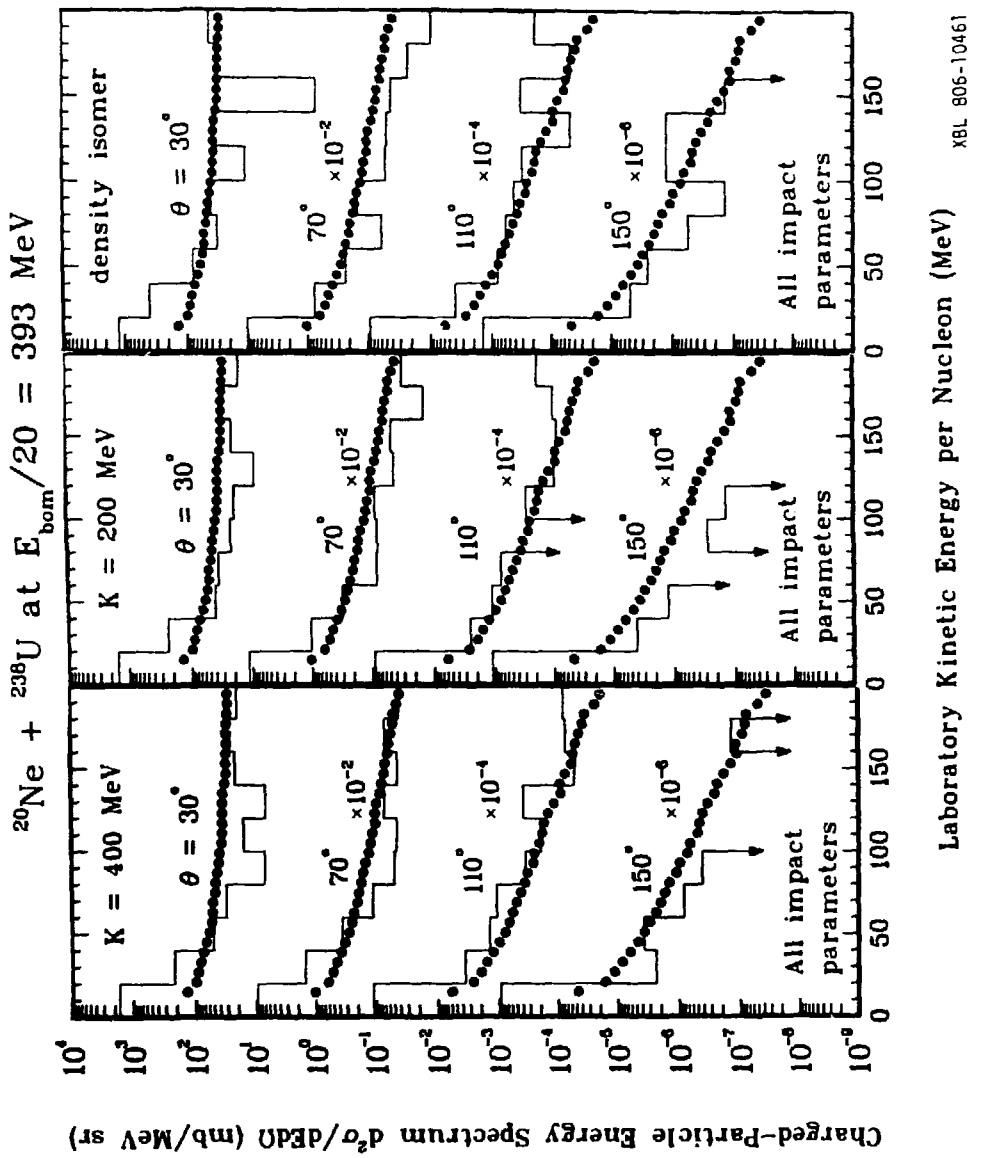
^{20}Ne + ^{238}U at E_{bom}/20 = 393 MeV
K = 400 MeV
K = 200 MeV
density isomer
θ = 30°
70°
110°
150°
×10⁻²
×10⁻⁴
×10⁻⁶
All impact parameters
Charged-Particle Energy Spectrum d²σ/dEdΩ (mb/MeV sr)
Laboratory Kinetic Energy per Nucleon (MeV)
XBL 806-10461

Fig. 7

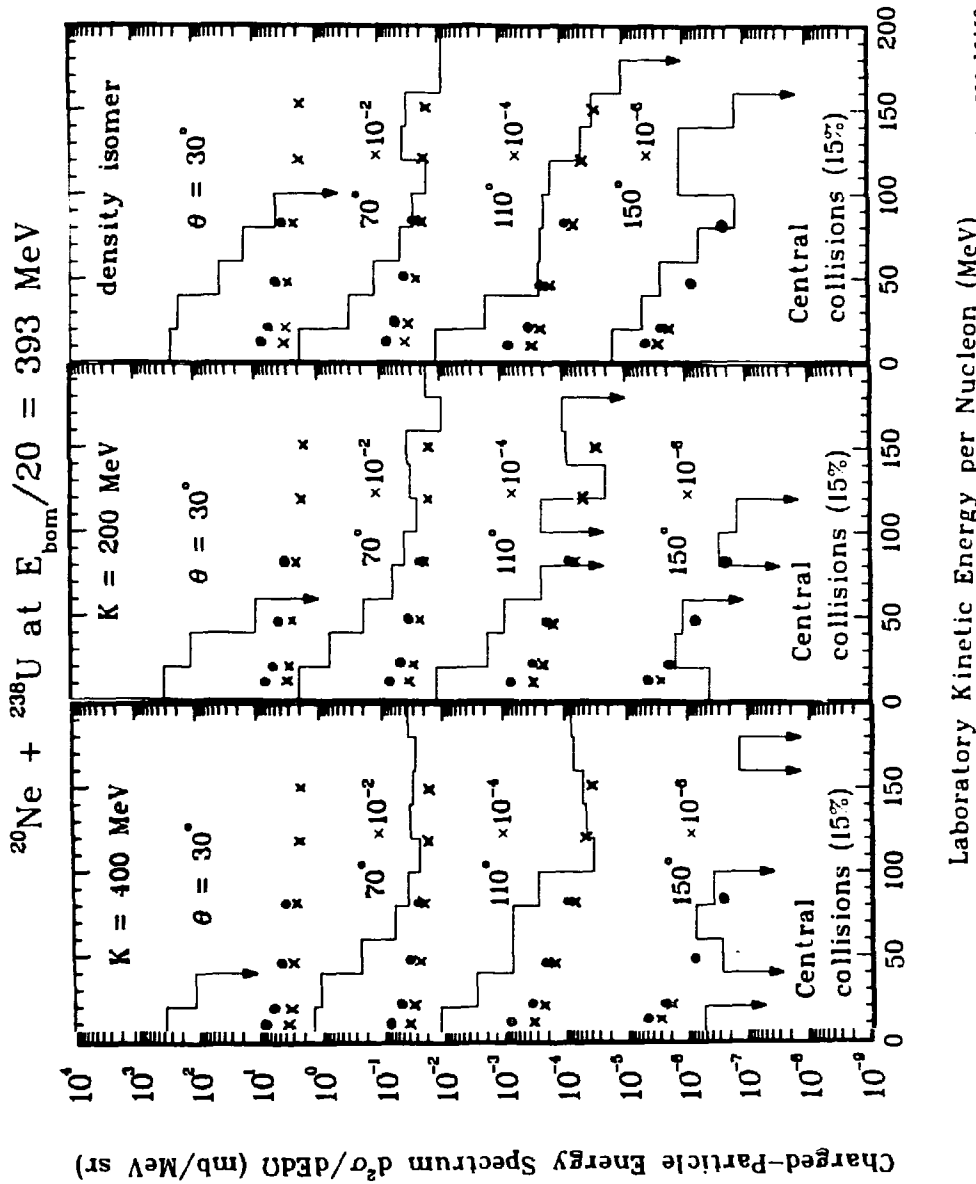
^{20}Ne + ^{238}U at E_{bom}/20 = 393 MeV
K = 400 MeV
K = 200 MeV
density isomer
θ = 30°
70° ×10⁻²
110° ×10⁻⁴
150° ×10⁻⁶
Central collisions (15%)
Charged-Particle Energy Spectrum d²σ/dEdΩ (mb/MeV sr)
Laboratory Kinetic Energy per Nucleon (MeV)
XBL 806-10460

Fig. 8

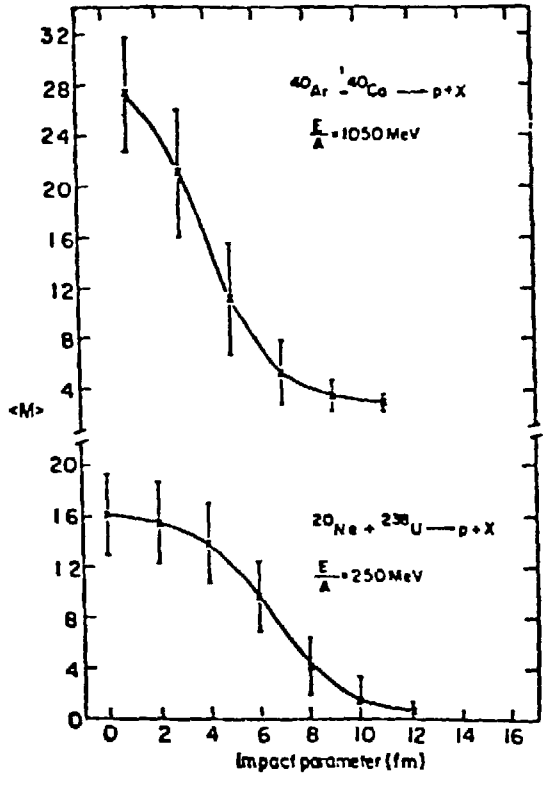

XBL 806-10459

Fig.9

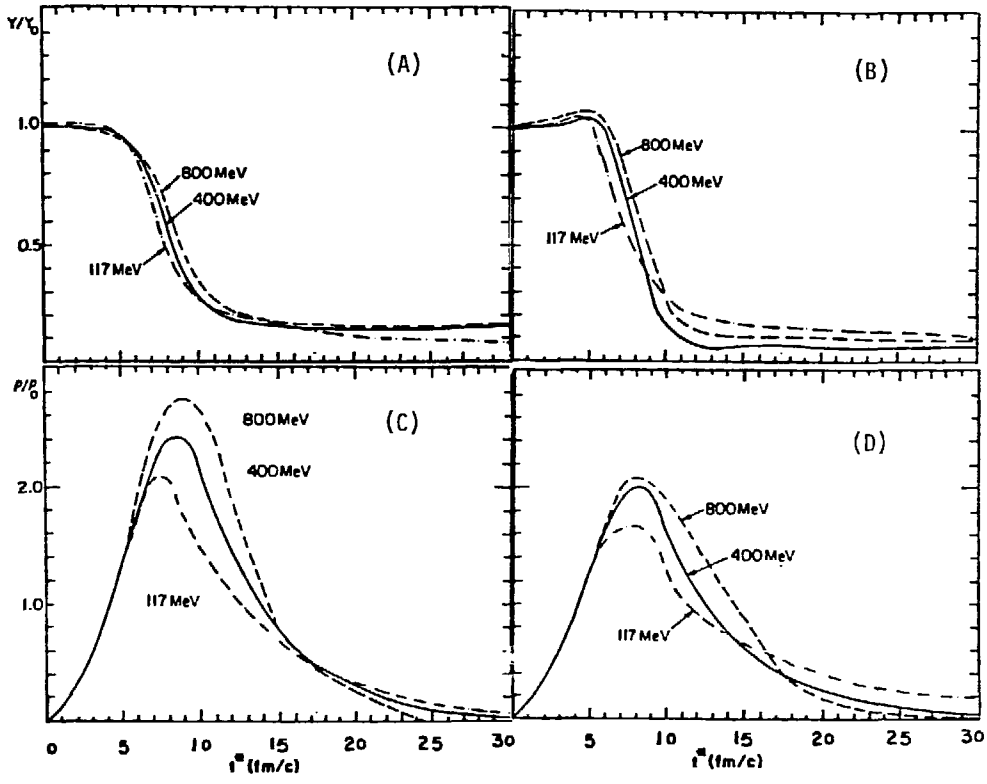

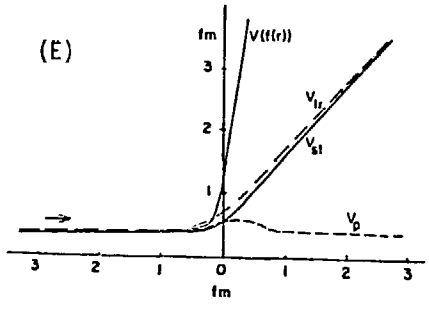

XBL 806-10458

Fig.10

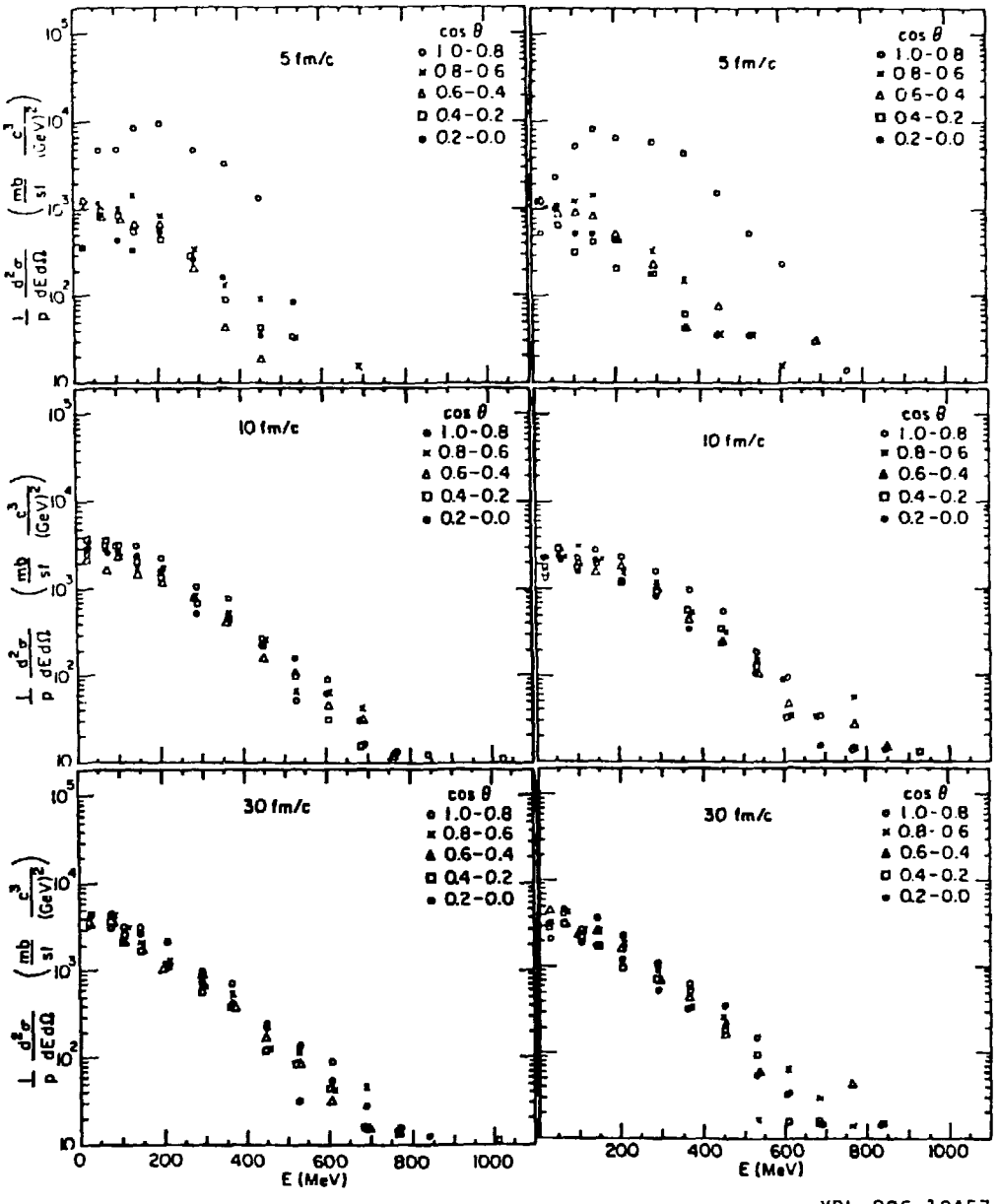

XBL 806-10457

Fig.11

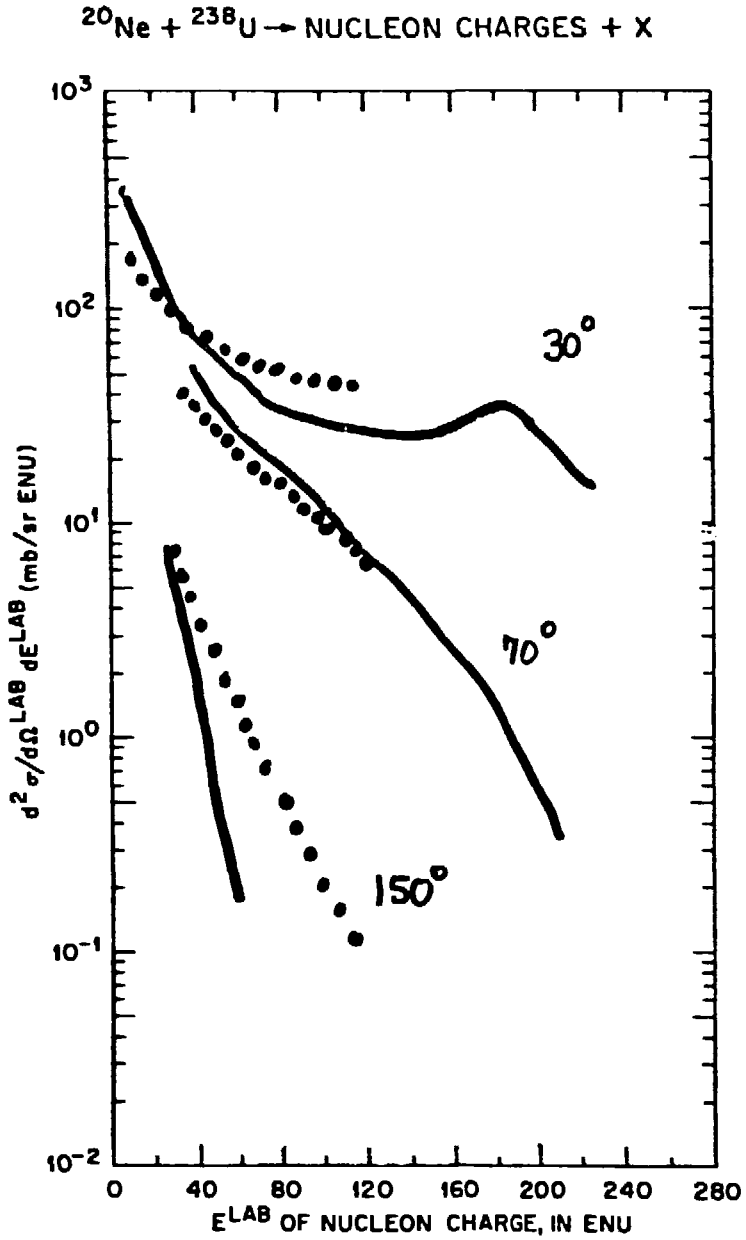

XBL 806-10456

Fig.12

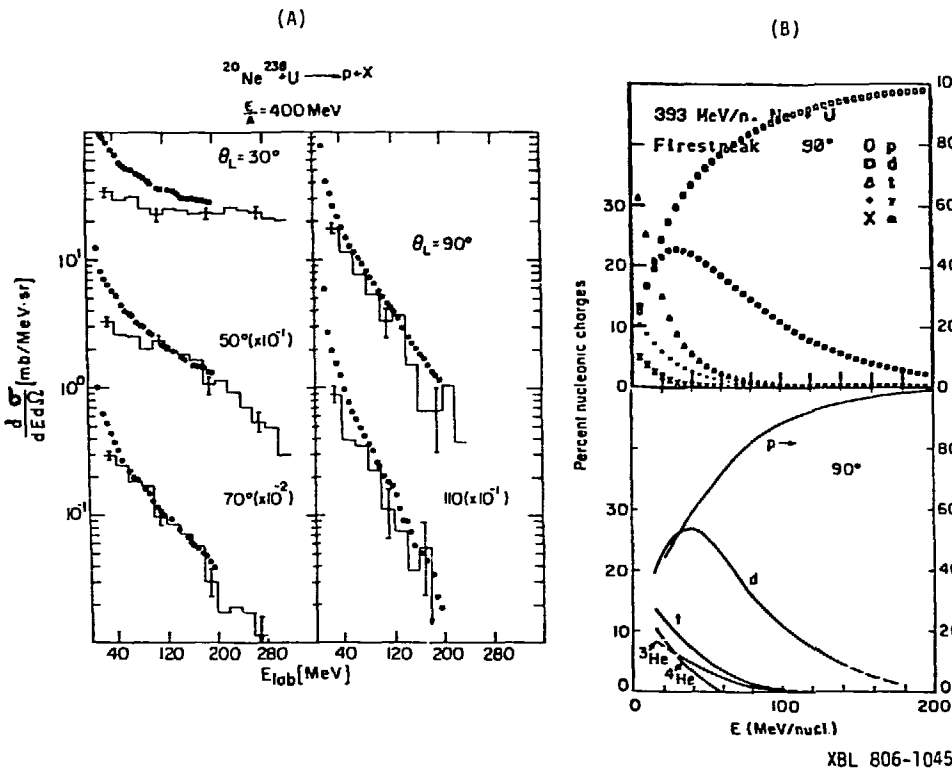
(A)
(B)
$^{20}Ne + ^{238}U \longrightarrow p + X$
$\frac{E}{A}$ = 400 MeV
θ_L = 30°
θ_L = 90°
50°(x10⁻¹)
70°(x10⁻²)
110(x10⁻¹)
$\frac{d\sigma}{dE\,d\Omega}$ [mb/MeV·sr]
E_{lab} [MeV]
393 MeV/n. Ne + U
First peak
90°
p
d
t
Percent nucleonic charges
E (MeV/nucl.)
XBL 806-10451

Fig.13

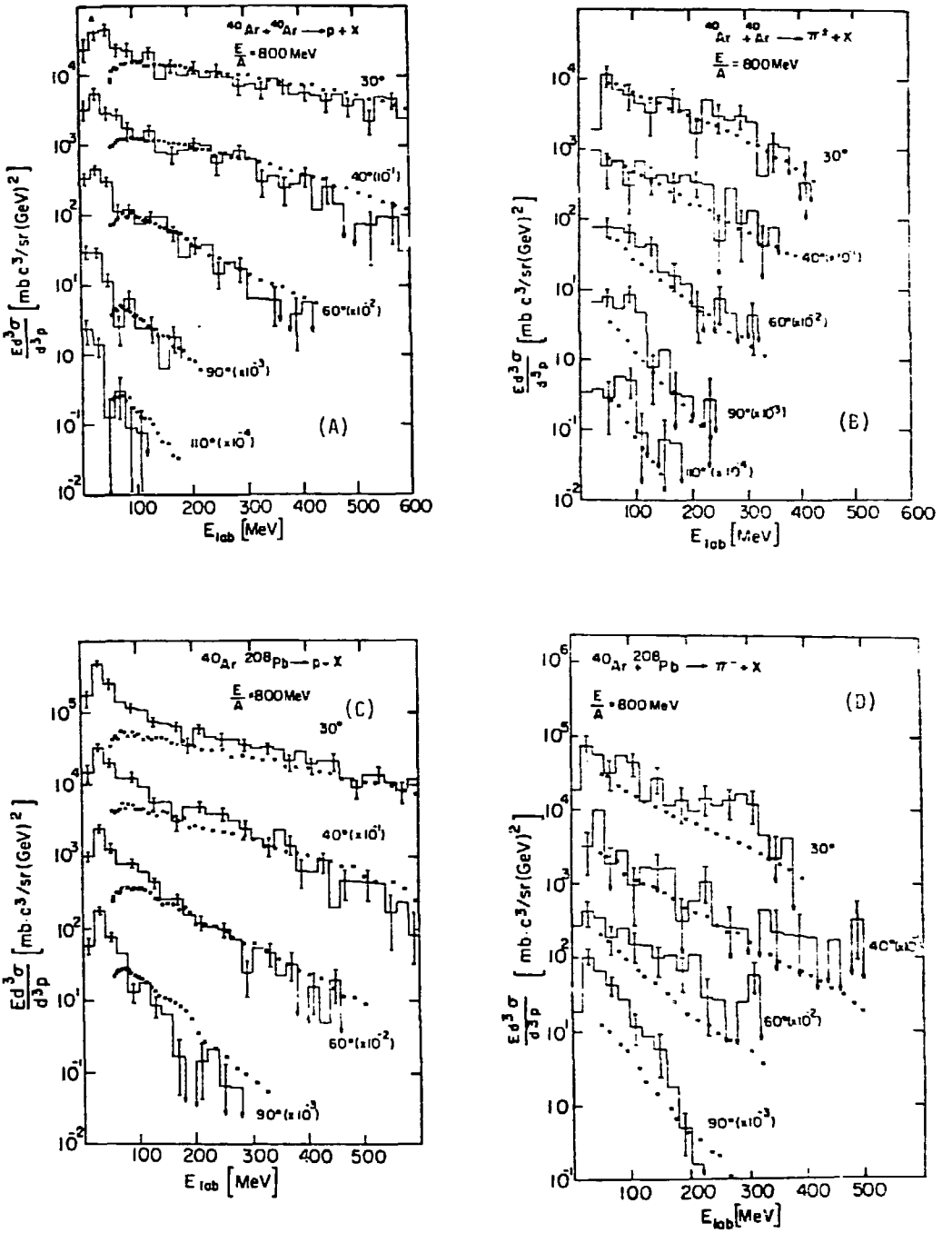

XBL 806-10452

Fig.14

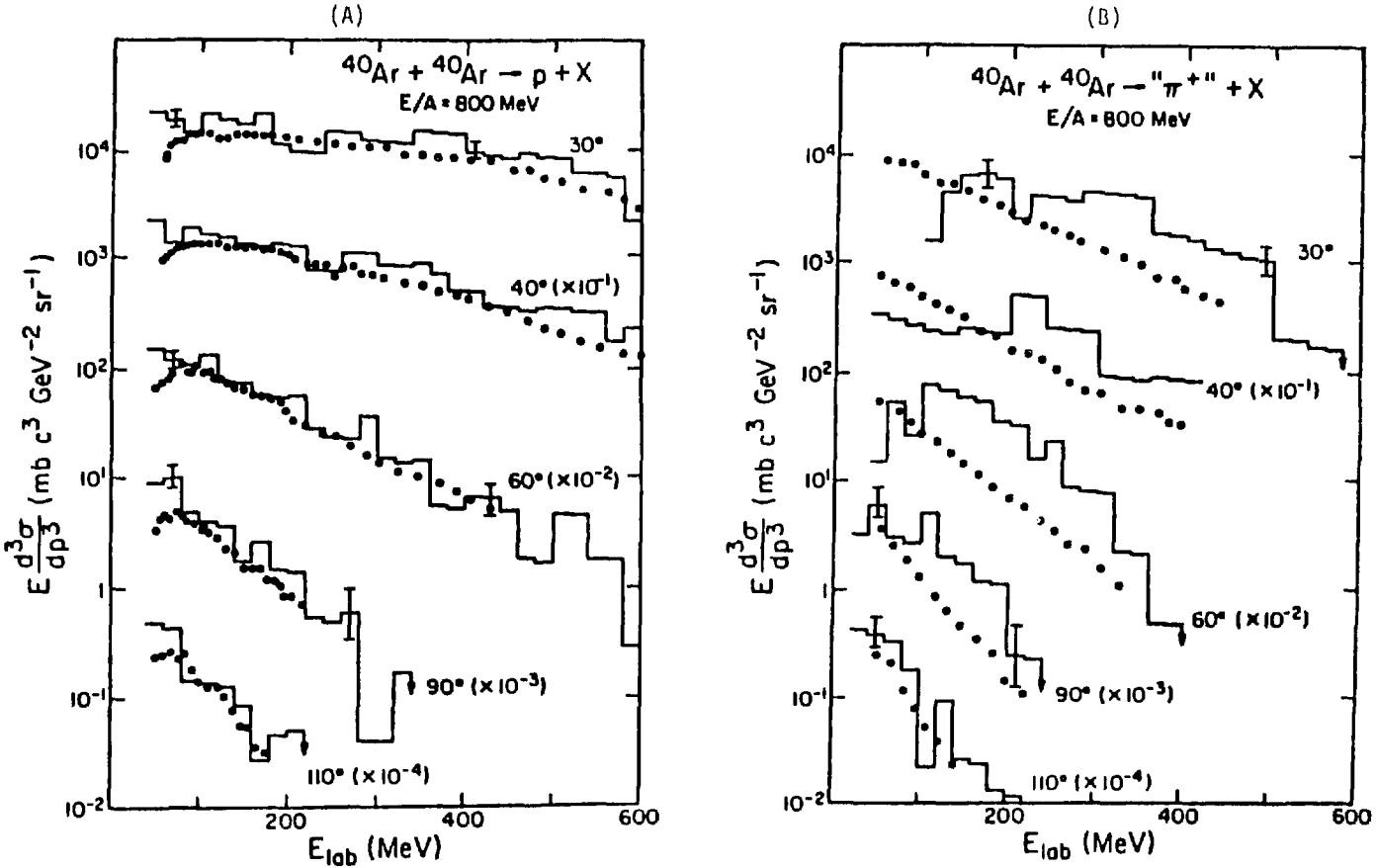

XBL 806-10454

Fig. 15

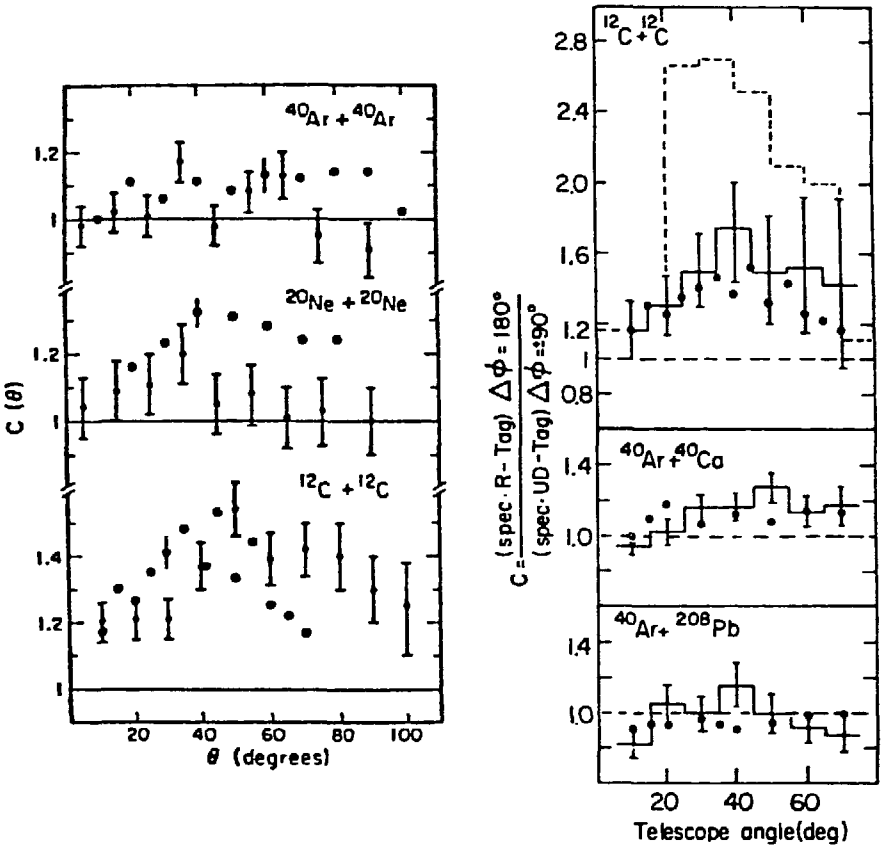

XBL 806-10450

Fig.16

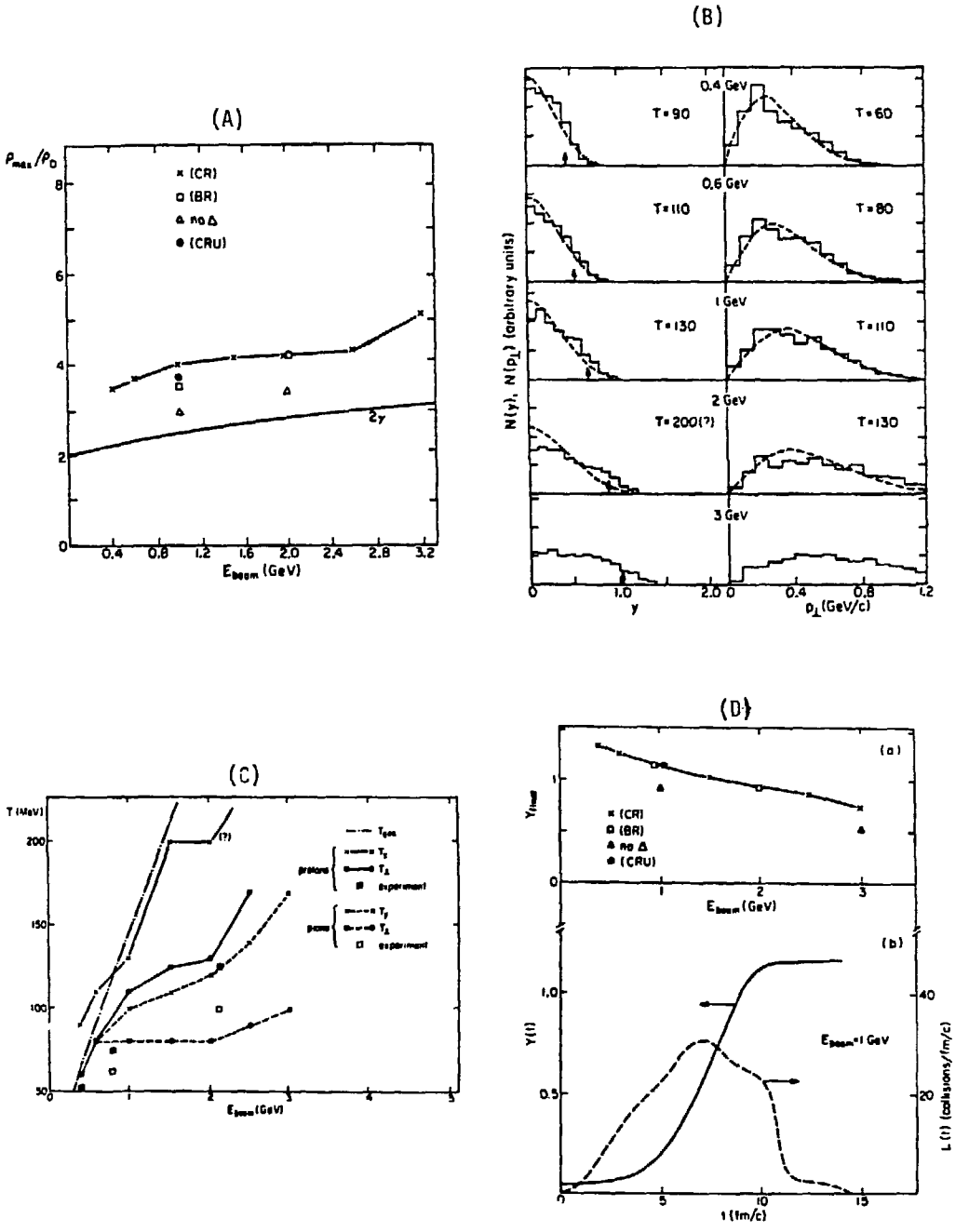
(A)
P_{max}/P_0
× (CR)
□ (BR)
△ no Δ
● (CRU)
2γ
E_{beam} (GeV)
(B)
0.4 GeV
T=90
T=60
0.6 GeV
T=110
T=80
1 GeV
T=130
T=110
2 GeV
T=200(?)
T=130
3 GeV
N(y), N(p⊥) (arbitrary units)
y
$p_\perp$ (GeV/c)
(C)
T (MeV)
(?)
protons
pions
experiment
E_{beam} (GeV)
(D)
(a)
Y_{final}
× (CR)
□ (BR)
△ no Δ
● (CRU)
E_{beam} (GeV)
(b)
Y(t)
E_{beam}=1 GeV
L (t) (collisions/fm/c)
t (fm/c)
XBL 806-10453

Fig.17

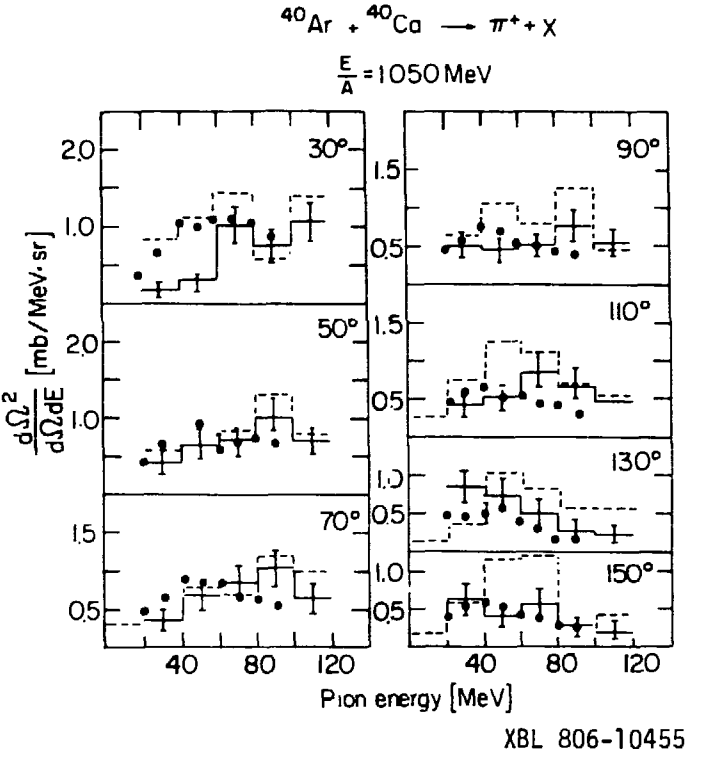
$^{40}Ar + ^{40}Ca \longrightarrow \pi^+ + X$
$\frac{E}{A} = 1050$ MeV
$\frac{d\Omega^2}{d\Omega dE}$ [mb/MeV·sr]
30°
50°
70°
90°
110°
130°
150°
Pion energy [MeV]
XBL 806-10455

Fig.18

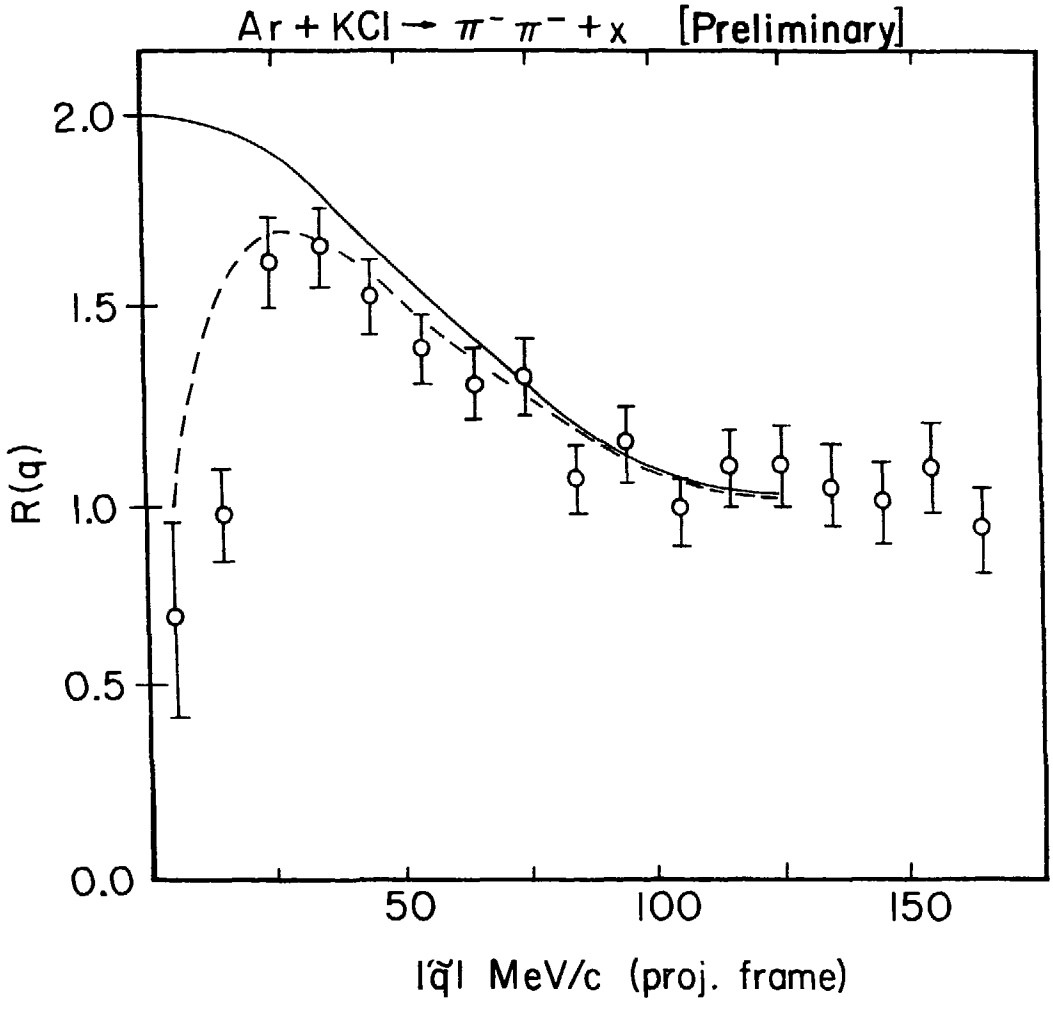

XBL 805-9727

Fig.19